NUMERICAL MODELING OF OBLIQUE PIPELINE–SOIL INTERACTION IN DENSE SAND

by

© MD Anan Morshed

A thesis submitted to the

School of Graduate Studies

in partial fulfillment of the requirements for the degree of

Master of Engineering (Civil)

Faculty of Engineering and Applied Science

Memorial University of Newfoundland

October 2019

St. John’s Newfoundland and Labrador Canada

Abstract

Buried pipelines are a safe, economical and efficient way of transporting oil and gas in both onshore and offshore environments. The pipeline generally passes through a wide variety of soil, and is buried at varying depths to maintain the flow of hydrocarbon by minimizing heat loss and avoiding interference with other human activities. Pipelines are usually installed in a trench and then backfilled with loose to medium dense sand. This backfill materials might be densified due to natural phenomena such as wave action at offshore shallow water depths. During operation, the pipeline might be subjected to loads resulting from oblique movement through the soil. The force/resistance due to relative displacement between soil and pipe during oblique movement is an important parameter for safe and economic engineering design. In the present study, an advanced numerical analysis is conducted to understand the pipe–soil interaction during oblique loading in dense sand. The Mohr–Coulomb (MC) and a Modified Mohr–Coulomb (MMC) are used for numerical analyses. Showing the limitations of the MC model, the advantages of the MMC model are shown for oblique loading cases. The importance of boundary conditions in the oblique loading analysis is shown. This study also focuses on the problems of current design practice where soil is represented as spring. It shows the importance of developing a new guideline for oblique loading, showing the limitation of ALA and PRCI guidelines. Large deformation finite element analysis is performed using the Arbitrary Lagrangian and Eulerian (ALE) method. The necessity of post-peak analysis is shown via yield surface formation for geohazard analysis. A parametric study is performed to show the effects of different oblique loading angles, diameters and embedment ratios on the force/resistance due to relative displacement between soil and pipe.

Acknowledgements

All praise to the Almighty, the Most Gracious, the Merciful and the Kind.

I would like to express my gratitude to my supervisor Dr. Bipul Hawlader, Professor, Memorial University of Newfoundland, Canada and co-supervisor Dr. Kshama Roy, Geotechnical Engineer and Pipeline Stress Specialist, Northern Crescent Inc., Canada for their continuous support, excellent guidance, motivation, patience, comments, remarks and engagement through the learning process of this dissertation. Without their guidance, this thesis would not have been possible.

I would also like to sincerely thank my colleagues, Dr. Sujan Dutta, Riyadul Arman, Shuvagoto Roy, Binoy Debnath, Diponkar Saha, Ripon Karamaker, Jin Chen, Rabindra Subedi, Rajith Dayarathne and Naveel Islam, for their invaluable advice, suggestion, assistance and time. Thanks to Dr. Rajib Dey, Tawsif Ahmed, Sabir Subedi and Suborno Debnath for their excellent suggestions, mental support and advices.

I am also indebted to my friends in St. John's, Newfoundland for their support, encouragement and exuberant memories. Special thanks Dr. Ashutosh Sutra Dhar, Tina Dwyer, Dr. Leonard M. Lye, Jerry Smith, Amy Holwell and all other the faculty and staff members in the Faculty of Engineering and Applied Science. Besides that, I want to thank the Teaching Assistant Union of Memorial University of Newfoundland (TAUMUN), Graduate Students' Union (GSU) and Engineering Graduates' Students Society (EGSS) to teach and help me a lot during my stay at MUN.

Finally, I would like to express my gratitude to my beloved parents, sibling and my lovely wife Shahreen Pea for their endless encouragement, strength, sacrifices, love and support. Their believe and support help me a lot to get into this position, and I strongly believe this is not the end, rather than a new beginning of my career as a geotechnical engineer.

This thesis is dedicated to them all.

Table of Content

List of Figures

List of Tables

Chapter 1

Introduction

1.1 Background and Motivation

Oil and gas are primary sources of energy. The revenue from oil and gas significantly impacts the economy of many countries. Canada is one of the leading oil and gas-producing countries in the world. After production, a safe and economical medium to transport oil and gas to the user is the main concern of government, regulatory agencies, and the oil industry. Pipelines are the most common medium of transporting oil and gas, although some other types of transportation, such as railway in onshore and tankers in offshore environments, are also used. Pipelines are considered as the most efficient, safest, and most reliable than other systems. According to the Canadian Energy Pipeline Association (CEPA), Canada has a network of approximately 117,500 km buried energy transmission pipelines that operates every day to transport oil and natural gas (http://www.cepa.com/).

Usually, pipelines are buried by excavating a trench and backfilling—in order to minimize the heat loss and maintain flow assurance. When granular materials such as sand are used for backfilling, the backfilled material is generally in loose to medium dense state. However, natural activities, including low-amplitude cyclic motion, such as wave action at shallow water depth in the offshore environment, could densify the soil (Clukey et al. 2005). Therefore, in order to capture pipe–soil interaction for a wide variation of density, researchers have done a great deal of analytical, experimental, and numerical modeling. Stuyts et al. (2016) showed the uncertainties in the estimation of uplift resistance of buried pipeline buried in sand of varying density (very loose to very dense) by compiling the available physical model test results and proposed analytical solutions.

The European Gas pipeline Incident data Group (EGIG) reported that ground movement represents the fourth major cause of gas pipeline failures, and about half of these cases resulted in pipeline rupture. The ground movements could cause the pipeline to move in different directions depending upon the orientation of the pipeline with respect to movement of soil. However, for simplicity, most of the previous studies have analyzed the pipeline–soil interaction for relative movement between pipeline and soil in three orthogonal directions, namely axial, lateral and vertical; and have assumed that the response of soil in one direction is not affected by the movement of soil in other directions. In other words, the soil springs in the three orthogonal directions, commonly used to model pipeline response, are independent. However, some researchers have identified some coupled effects (Guo 2005; Cocchetti et al. 2009; Daiyan 2013). When the pipeline does not move along a purely vertical or purely later direction, rather moves along an inclined direction on a vertical plane, the response is governed by both the lateral and uplift resistances of soil. Also, if the pipeline is buried in dense sand, the response becomes further complicated because dense sand has a post-peak softening in the stress–strain behavior. Therefore, an appropriate soil constitutive model that properly captures the stress–strain behavior of sand for varying densities, and a numerical technique that can model such behavior, is required for pipeline–soil interaction analysis. In the present study, pipeline–soil interaction in dense sand for oblique loading in a vertical plane (i.e., vertical upward and lateral) is modeled numerically.

1.2 Scope of the Research

Pipeline response is generally analyzed using three nonlinear springs (Fig 1.1). When a pipeline is subjected to any two of the lateral, axial and upward loadings, it displaces in an oblique direction. In the field, the following three types of oblique loadings might occur: (i) lateral–vertical, (ii) lateral–axial, and (iii) axial–vertical (Fig 1.2). The present study focuses on the oblique lateral–vertical

interaction. However, the author understands that the other two types of oblique loading are equally important in pipeline design. The modeling is performed for pipelines buried in dense sand.

1.3 Objectives

The main objectives of the present study are:

- Develop finite element (FE) models that can successfully capture the oblique loading (lateral–vertical);
- Develop a yield surface for oblique loading for varying different boundary conditions;
- Identify the importance of post-peak softening of dense sand in the pipe–soil interaction analysis;
- Identify the role of progressive failure mechanisms and shear band formation on soil resistance;
- Conduct a parametric study for varying diameter, embedment ratio, and oblique angle; and
- Present the limitations of existing design guidelines for oblique loading.

1.4 Outline of the Thesis

This thesis is prepared in manuscript format. The outcome of the study is presented in five chapters.

Chapter 1 highlights the background, scope, and objectives of the research work.

Chapter 2 presents a general literature review. As the thesis is prepared in manuscript format, the problem-specific literature reviews are provided in Chapters 3–4.

Chapter 3 presents finite element analysis of oblique loading of buried pipelines in dense sand. This chapter has been published as a technical paper in the 71st Canadian Geotechnical Conference, GeoEdmonton 2018, Edmonton, Alberta, Canada, September 23–26, 2018.

Chapter 4 presents the yield surface, effect of post-peak softening and parametric studies. This chapter is prepared as a manuscript to submit in a journal.

Chapter 5 summarizes the outcomes of the research and recommendations for future studies.

As the thesis is prepared in manuscript format, the references cited in Chapters 3–4 are listed at the end of these chapters, and the references cited in Chapters 1, 2 are listed in the “Reference” section at the end of the thesis.

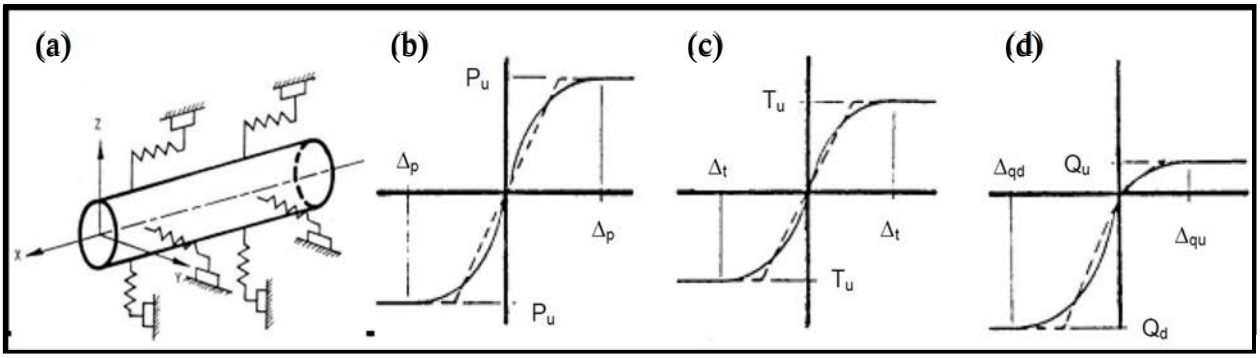

Figure 1.1 (a) Idealized pipe–soil interaction with discrete springs, (b) Lateral loading, (c) Axial loading, and (d) Upward loading (ALA 2005)

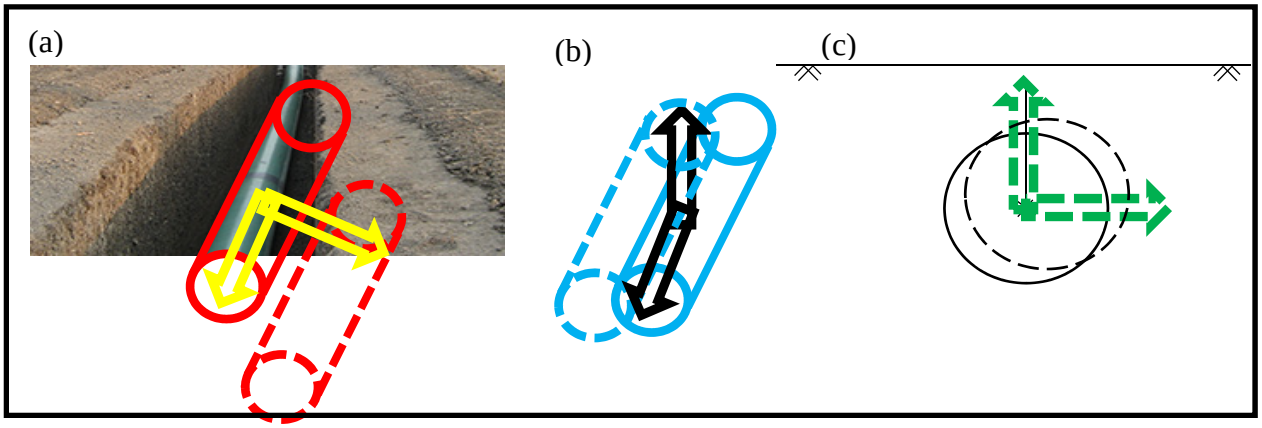

Figure 1.2 (a) lateral–axial, (b) axial–vertical and (c) lateral–vertical oblique loadings

Chapter 2

Literature Review

2.1 Introduction

As the thesis is written in manuscript format, a chapter specific literature review is presented in Chapters 3–4. The primary purpose of adding this chapter is to present an additional review of available studies relevant to the present research. Where needed figures are added for a better comparison and for providing further information about previous studies, which could not be included in the manuscripts because of space limitation. The literature review presented in this chapter covers the behavior of pipes buried in dense sand for lateral–vertical oblique loading. Besides introducing current engineering practice, terminologies and definitions, this chapter highlights the potential causes of oblique loading, the modeling technique and the results of some previous studies. Finally, the limitations of current design guidelines for oblique loading of pipeline in dense sand are presented.

2.2 Current Engineering Practice

Buried pipelines are extensively used to transport water and hydrocarbons. Generally, a pipeline traverses through a variety of soils and terrain, sometimes over thousands of kilometers. Geohazards and the associated ground movement represent a significant threat to pipeline integrity that may result in pipeline damage and operational interruption. Safe, economical and reliable operation of pipeline transportation systems is the primary goal of pipeline operators and regulatory agencies. Therefore, it is important to accurately evaluate soil resistance or loading on pipelines in response to the relative movement of surrounding soils, which could be a primary cause of failure.

In the current engineering practice, the structural response of a pipeline is generally evaluated by modeling the pipeline as a simplified beam. The response soil to the deformation of the pipeline is modeled using three sets of soil springs in the axial (longitudinal), transverse horizontal, and transverse vertical directions. The response of these soil springs in the three orthogonal directions is independent, which means that the deformation of soil in one direction does not affect pipe–soil interactions in the other two directions. The general form of the load–displacement relations for these springs can be expressed as:

$$T = f(x);\ P = f(y);\ Q = f(z) \tag{2.1}$$

where T, P and Q are the soil loads applied to unit length of the pipeline, and x, y and z are the relative displacements between the pipe and surrounding soil in the longitudinal, lateral and vertical directions, respectively.

2.3 Causes of Oblique Loading

Buried pipelines might be subjected to oblique loadings from different sources. Among them, the ground movement is a common one. Ground movement can occur in various forms—some of them are rapid (e.g., landslides) while some of them are slow (e.g., creep movement of soil near the river bank). Failure of the slope might be triggered by many sources such as natural activities (e.g., earthquake and erosion near the river bank) or human activities (e.g., oversteeping, surcharge). Such ground movement will not always cause a purely axial, lateral, or vertical loading; instead, many sections of the pipeline might experience oblique loading. Figure 2.1 shows the failure of the pipeline after the 1988 Tennant Creek earthquake in Australia. This ground movement resulted in an oblique displacement of the pipeline that shut down this gas pipeline. Again, pipelines might need to cross some fault zones along its route. Even though most fault displacement is confined to a narrow zone, the potential for pipeline damage is high due to the large strains impose on the pipe (Eidinger et al. 2002). Ha et al. (2008) discussed different types of faulting (Fig. 2.2)

and their effect on the pipeline during permanent ground deformation (PGD). The combination of these faults and PGD might lead the pipe to move in an oblique direction. Unless the movement of the soil occurs very rapidly, the soil response during pipe–soil interaction in sand can be modeled as drained condition because of the high permeability of sand.

2.4 Previous Studies

Nyman (1984) developed an analytical solution for estimation of ultimate soil restraint of pipeline subjected to oblique lateral–vertical loading. The solution was developed assuming the pipeline analogous to anchor plates. It was suggested that the maximum oblique force (F_{uo}) could be calculated using a rectangular hyperbolic function of oblique loading angle with the vertical (α) and the ultimate lateral (F_{uh}) and vertical (F_{uv}) restraints. For a tentative design, a bilinear load–displacement relationship is suggested where the lower bound soil parameters should be used to compute soil resistance and upper bound values yield displacements. To calculate F_{uh} and $F_{uv,}$ the empirical equations proposed by Audibert and Nyman (1977) and Vesic (1969), respectively, were recommended. Later, a large volume of research was conducted on lateral and vertical uplift resistance for pipelines and anchors buried in sands and clays (Trautmann 1983; Yimsiri et al. 2004; Cheuk et al. 2008; White et al. 2008; Roy et al. 2016, 2018a,b). These studies include full-scale tests, small-scale laboratory and centrifuge tests, and numerical analysis. Compared to the number of studies on lateral and vertical uplift resistances, the research on oblique loading is limited. Hsu (1996) conducted physical experiments to investigate the restraint of soil against the vertical–lateral oblique motion of the pipelines of 38.1 mm – 228.6 mm diameter buried in dry loose sand at embedment ratios (H/D) of 1.5 and 3.0, where H is the depth of the center of the pipe. The normalize force ($F_o/\gamma HDL$, where F_o is the oblique load, γ is the unit weight of soil, and L is the length of the pipe segment) and normalized displacement (y/D, where y is the oblique displacement) relationships can be

represented as a hyperbolic function. It is also found that the soil restraint primarily increases for an oblique angle $\alpha = 45° – 90°$. Later, Hsu and his co-workers conducted experimental studies also on longitudinal and transversal oblique loading conditions for loose and dense sands (Hsu et al. 2001; Hsu et al. 2006). However, as the focus of the present study is on lateral–vertical oblique loading, these studies are not discussed in detail.

Calvetti et al. (2004) conducted physical and numerical modeling of pipeline–soil interaction for vertical–lateral oblique loading cases. For physical modeling, tests were conducted in a 0.8 m × 0.5 m × 0.3 m box filled with Hustan rf sand in loose condition. For numerical modeling, a distinct element method was used. Based on physical and numerical modeling, an interaction diagram for the maximum oblique loading varying from vertical upward to vertical downward ($\alpha = 180°$) is developed. The numerical analyses provide the soil failure mechanisms and load transfer to the soil.

Di Prisco and Galli (2006) conducted a series of small-scale tests where the pipe was buried at embedment ratio from 1.5–3.5 in loose and dense Ticino sand and then pulled laterally, vertically, and also at 45° angle with vertical. Finite element simulations were also performed to understand the mechanisms further. However, in their FE simulation, the post-peak softening behavior was not considered instead a constant friction angle of 42° was used.

Cocchetti et al. (2009) conducted numerical analyses to model the behavior of pipe–soil interaction under the combined vertical–horizontal loading scenario. The pipe was discretized by a series of three-dimensional beam finite elements, and the pipe–soil interaction was modelled by microelement theory. The proposed approach captured the coupling among the different loading components.

Daiyan et al. (2011) presented the results of centrifuge tests and numerical analysis to understand the behavior of axial–lateral oblique loading of pipelines buried in dense sand. The predicted ultimate loads from numerical simulations were consistent with the centrifuge data. A parametric study was conducted for soil friction angle, pipe–soil interface resistance, and burial depth. It was shown that, with the increase of soil friction angle and burial depth, the lateral and axial interaction factors increase proportionally with oblique angles.

Roy and Hawlader (2012) presented FE analysis to understand better the complex pipe–soil interaction and load transfer mechanisms during combined axial–lateral loading. They used the Mohr-Coulomb failure criterion to model sand behavior and showed the necessity of using an advanced soil constitutive model to overcome the limitation of the Mohr–Coulomb model in pipeline–soil interaction modeling. Daiyan (2013) investigated the complex soil failure mechanisms during oblique pipeline–soil interactions events associated with large permanent ground deformation. A series of centrifuge tests and a three-dimensional continuum finite element modeling was performed to better understand this event. Interaction diagrams that characterized the coupled soil load–displacement mechanisms were developed in this study. Farhadi Hikooei (2013) used Abaqus finite element software to model oblique loading for both sand and clay. This study focused on the maximum dimensionless oblique force, and failure envelopes were developed which are similar to Guo (2005) for pipelines in clay.

Monroy-Concha (2013) conducted physical experiments for oblique lateral–vertical loading of pipelines buried in dense and loose sands. The tests conducted under displacement-controlled loading condition and showed the post-peak response at large displacement. Fenza (2016) conducted full-scale tests and numerical analyses to examine the lateral pipeline–soil interaction events with both constrained and unconstrained uplifting of the pipe buried in sand and showed higher resistance in the former one. Jung

et al. (2016) presented large-scale test results on dry and partially saturated sands. They conducted finite element analysis for varying oblique loading angles of 0–180° (i.e., from vertical upward to vertical downward). In numerical modeling, they also considered the effects of suction in the partially saturated soil. Debnath (2016) did physical modeling using a geotechnical centrifuge to improve the current understanding of soil load coupling effects of buried pipelines in loose and dense sands. The tests were conducted for shallow buried depths by pulling a section of pipe at different oblique angles in the axial–lateral plane. The results are consistent with previous physical modeling (Daiyan 2013) and numerical simulations (e.g., Daiyan et al., 2011; Daiyan, 2013). Wijewickreme et al. (2017) conducted full-scale tests on a 400-mm diameter pipeline buried in moist sand and crushed limestone. The oblique loading was applied in the lateral-vertical upward plane. It is found that the peak soil restraint depends on the peak friction angle when the oblique loading is applied at an angle closer to the horizontal. Marcotte (2018) conducted a series of physical model tests to investigate oblique loading effects, in the lateral–axial plane, on buried pipes in cohesionless soil**.** The failure surfaces obtained from the test results at the yield were compared with previous physical model tests and showed a good correlation.

The oblique loading response of pipelines buried in clay was also invested in previous studies. Guo (2005) conducted FE analysis using an elasto-plastic model for clay and developed a failure envelope for oblique loading. In order to accommodate large deformation in FE analysis, Pike and Kenny (2011) used a coupled Eulerian–Lagrangian (CEL) approach to analyze the vertical–lateral oblique loading problems. A detailed review of previous studies on the pipeline in clay is not presented here because the focus of the present study is the modeling of pipeline buried in sand.

A summary of the available studies on oblique pipe−soil interaction is presented in Table 2.1.

2.4.1 Lateral–vertical oblique loading in inclined anchors

A number of studies used to response of strip anchor to analyze the behavior of pipeline assuming that there is similar behavior between these two structures (Fig. 2.3).

Different types of soil failure mechanisms have been proposed to evaluate the ultimate pullout capacity of the anchor, which can be considered the ultimate soil resistance for pipelines. Figure 2.4 show two proposed failure mechanisms for inclined anchors in sand. The formation of the failure wedge influences the pullout capacity, which has been investigated using finite element (Rowe and Davis 1982; Dickin and King 1993) and finite element limit analysis (Bhattacharya and Kumar 2013).

Most of the previous numerical studies modeled the drained behavior of sand using the conventional Mohr–Coulomb model by giving the constant values of friction angle (ϕ') and dilation angle (ψ). However, experimental studies show that ϕ' and ψ depend on loading, relative density, mean effective stress, and more importantly, the strain level. A pipeline/anchor might move considerably large distance before mobilizing the maximum soil resistance or the pullout capacity. Therefore, the soil elements along the failure plane of the failed soil wedge undergo considerably large strain, and these elements will have post-peak softening. For lateral and vertical loading of pipelines and anchors, these factors have been considered in modeling of dense sand in finite element simulation (Jung et al. 2013, Roy et al. 2016, 2018, Pike 2016). It has been shown that these factors change the failure pattern and ultimate soil resistance both in lateral and vertical directions.

2.5 Current Guidelines

ALA (2005) and PRCI (2009) are the most commonly used guidelines for the design of buried pipelines. For structural analysis of pipelines, the force–displacement relationship is generally given by a set of independent springs in the three orthogonal axes where the spring behavior is defined by bilinear or

hyperbolic functions. However, the recommendations for calculating the peak (maximum) oblique resistance is missing in both guidelines. The summary of the current guidelines is highlighted for vertical uplift and lateral soil springs.

- The ALA (2005) gives a significantly high lateral resistance compared to other guidelines and empirical equations (Roy 2018b). However, the use of a higher resistance is generally conservative in terms of the structural response of a pipeline, because the force on the pipeline is higher for a given lateral displacement (O'Rourke and Liu 2012).
- PRCI (2009) recommendations are based on FE results presented by Yimsiri et al. (2004), which have been calibrated against Trautmann's (1983) physical test data. Therefore, the peak dimensionless force versus the embedment ratio curve proposed by the PRCI (2009) is very close to Trautmann and O'Rourkes' (1985).
- ALA (2005) and PRCI (2009) did not consider the effects of pipe diameter on the dimensionless vertical or lateral force.
- The mentioned guidelines recommend the use of peak resistance, even at displacements greater than required to mobilize the peak value. However, in physical model tests of pipes buried in dense sand show a reduction of resistance after the peak, both for lateral and upward loading (Trautmann 1983; Chin et al. 2006; Cheuk et al. 2008; Burnett 2015). DNV (2007) recognizes the importance of post-peak reduction of soil resistance for upheaval buckling of buried pipelines and Randolph (2012) also mentioned the importance of post-peak reduction of soil resistance for lateral buckling of offshore pipelines.

2.6 Summary

The literature review presented in this chapter shows that several factors such as stress–strain behavior of soil, pipe diameter, and embedment ratio affect the soil resistance on pipelines buried in sand. Most of the previous studies and current guidelines focus on the peak resistances, even for the pipelines buried in dense sand, and do not consider the effect post-peak reduction of soil resistance. Moreover, numerical studies using typical finite element programs might have suffered from numerical issues related to mesh distortion at large displacements. In this study, a FE modeling technique is used that can simulate large displacements, which also provides a better insight into the effects of strain-softening behavior of soil and reduction of cover depth with displacement of the pipeline on oblique resistance.

Figure 2.1 Failure of the pipeline after the 1988 Tennant Creek earthquake in Australia (from Geoscience Australia)

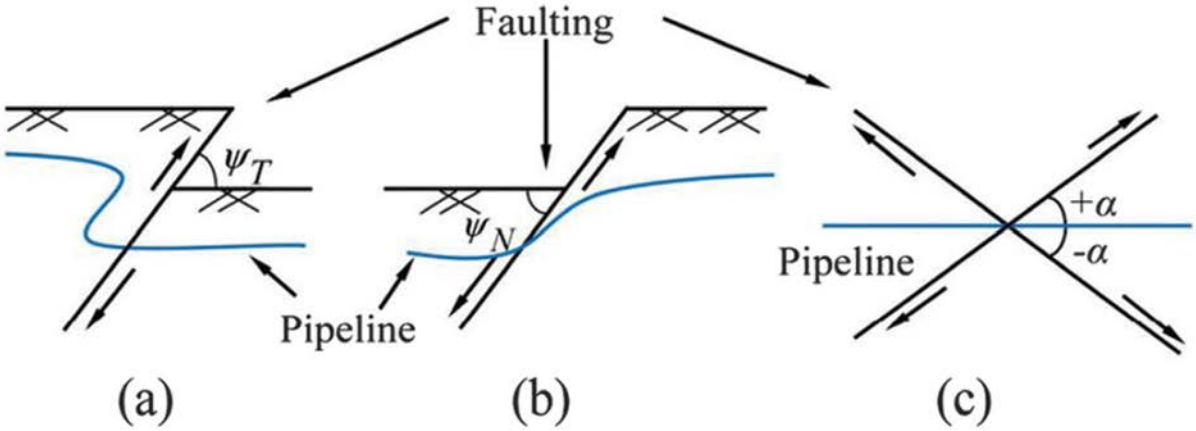

Figure 2.2 Different fault types and their effect on pipelines: (a) reverse fault (b) normal fault and (c) strike-slip fault (adapted from Ha et al. 2008).

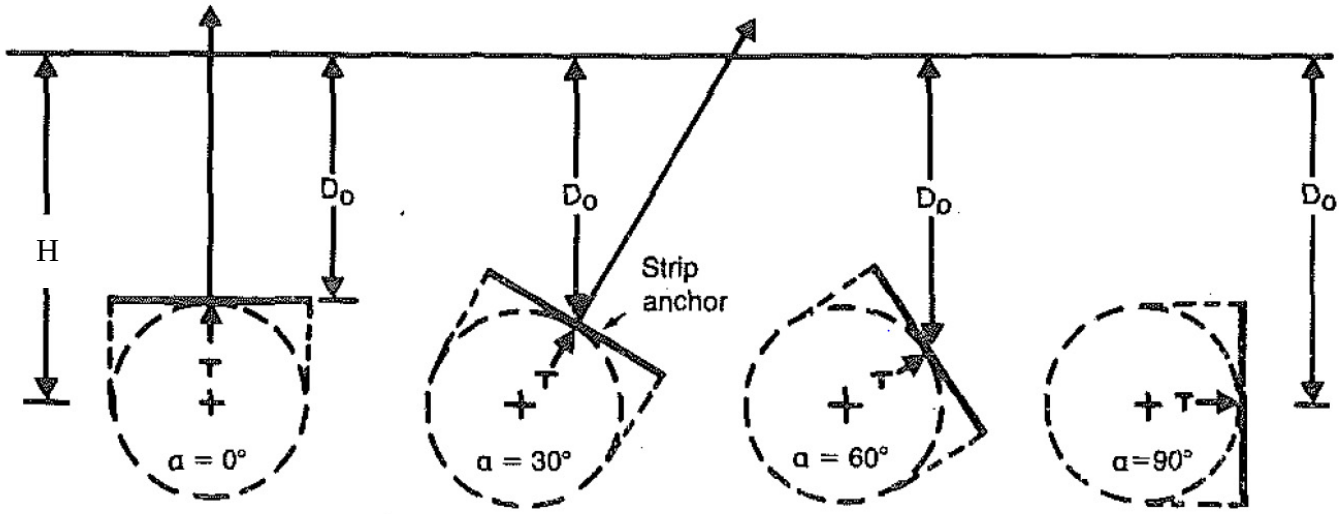

Figure 2.3 Analogy between anchor and pipeline (Nyman 1984)

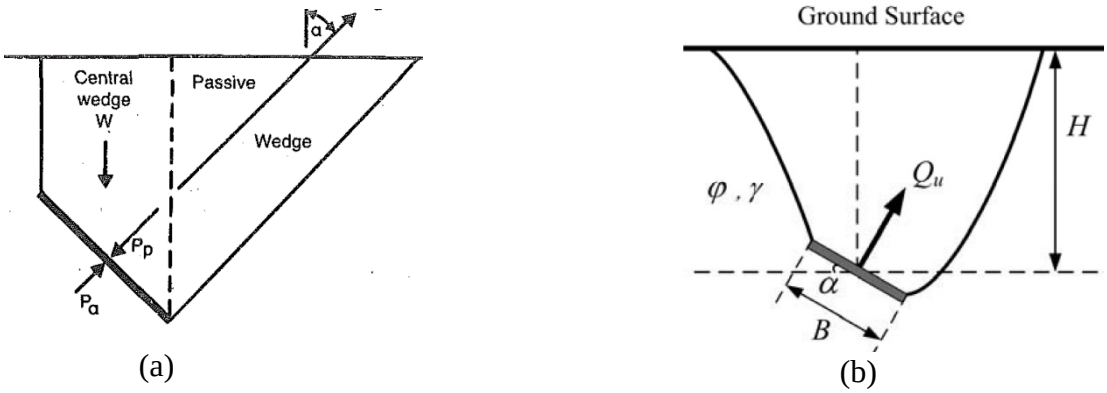

(a) (b)

Figure 2.4 Idealized soil failure mechanism: (a) Meyerhof (1973); (b) Yu et al. (2014)

Table 2.1 Summary of previous studies on oblique pipe–soil interaction

Reference	**Study Type**	***H*/*D***	**Pipe Diameter (mm)**	**Relative Density, D_R (%)**	**Remarks**
Nyman (1984)	Analytical	1.5, 3.5	–	–	Loose and dense sand, lateral–vertical oblique loading
Hsu (1996)	Large-scale (experimental)	1.5, 3.5	38.1, 76.2, 152.4, 228.6	21	Steel pipe, loose sand, axial–lateral oblique loading
Zhang et al. (2002)	Centrifuge test (experimental)	–	1000	–	Calcareous Sand, lateral–vertical oblique loading
Calvetti et al. (2004)	Both small scale (experimental) and numerical	3.5	20, 50	–	Loose sand, lateral–vertical oblique loading
Guo et al. (2005)	Numerical analysis	1.03, 1.34 1.97, 3.03, 6.18	330, 950	–	Clay soil, lateral–vertical oblique loading
Hsu et al. (2006)	Large-scale (experimental)	1.5,3.5	152.4, 228.6, 304.8	94	Steel pipe, dense sand, axial–lateral oblique loading
Di Prisco and Galli (2006)	Small-scale experimental and numerical	1.5,2.5, 3.5	50	37.2, 100	Dry Ticino sand, lateral–vertical oblique loading

Reference	Study Type	*H*/*D*	Pipe Diameter (mm)	Relative Density, D_R (%)	Remarks
Hodder and Cassidy (2008)	Centrifuge test (experimental)	–	10	–	Clay soil and lateral–vertical oblique penetration
Cocchetti et al. (2009)	Numerical analysis	1.5 (2D analysis) 3 (3D analysis)	750 (2D analysis) 500 (3D analysis)	–	Dense sand, lateral–vertical oblique loading
Daiyan et al. (2011)	Both Centrifuge test (experimental) and numerical analysis	2	504	82	Steel pipe, dense sand, axial–lateral oblique loading
Pike and Kenny (2011)	Numerical analysis	2, 6	400, 1000	–	Clay and lateral–vertical oblique loading
Roy and Hawlader (2012)	Numerical analysis	3	102	81	Steel pipe, dense sand and lateral–axial oblique loading
Daiyan (2013)	Numerical analysis	2,4,7	504	82	Steel pipe, dense sand, axial–lateral and lateral–vertical oblique loading
Farhadi Hikooei (2013)	Numerical analysis	1.5, 3.03, 4.5, 6	950	–	Steel pipe, dense sand, clay and lateral–vertical oblique loading
Monroy-Concha (2013)	Full scale (experimental)	1.6, 1.9	406.4, 457	–	Steel pipe, loose and dense sand, lateral–vertical oblique loading
Fenza (2016)	Both full scale experimental and numerical	1.5–11	102, 457	20–40	Loose and medium dense sand, lateral–vertical oblique loading

Reference	Study Type	H/D	Pipe Diameter (mm)	Relative Density, D_R (%)	Remarks
Jung et al. (2016)	Numerical analysis	3.5–100	102–900	–	HDPE pipe, medium, dense and very dense sand, lateral–vertical oblique upward and downward loading
Debnath (2016)	Centrifuge test (experimental)	2	609	32.2, 33.6, 74.5, 75	Steel pipe, loose and dense sand, axial–lateral oblique loading
Wijewickreme et al. (2017)	Full scale (experimental)	1.6	400	–	Steel pipe, dense sand and lateral–vertical oblique loading
Marcotte (2018)	Centrifuge test (experimental)	2, 4	304, 609.5	32	Steel pipe, loose sand, axial–lateral oblique loading

Chapter 3
Numerical Modelling of Oblique Pipe–Soil Interaction in Dense Sand

Co-Authorship: This chapter has been published in a conference as a technical paper as: Morshed, M.A., Roy, K., Hawlader, B.C. and Dhar, A.S. (2018), 'Numerical Modelling of Oblique Pipe–Soil Interaction in Dense Sand'. Most of the research in this chapter has been conducted by the first author. The other authors mainly supervised the research and reviewed the manuscript.

Abstract

Pipe–soil interaction during large ground displacements is typically simulated using nonlinear soil springs aligned in three orthogonal directions with respect to the longitudinal axis of the pipeline. However, recent studies have indicated that in the complex pipe–soil interaction events (e.g., lateral–vertical direction), assuming no interaction between the loads applied to the pipeline in different directions does not truly represent the field condition and therefore, an advanced numerical modeling is required. Finite element (FE) analysis of oblique (lateral-vertical) pipe–soil interaction for pipe buried in dense sand is presented in this paper. Two soil constitutive models, the Mohr–Coulomb (MC) model with constant angles of internal friction and dilation, and a Modified Mohr–Coulomb (MMC) model with pre-peak hardening, post-peak softening, density and confining pressure dependent friction and dilation angles, are considered. The FE analyses are performed using the Arbitrary Lagrangian Eulerian approach available in Abaqus/Explicit FE software. Results show a significant difference in the peak oblique resistance for different loading angles. Shear band formation due to strain localization for different loading angles is discussed from the simulations with both the

MC and MMC models. FE results show that the MMC model can better simulate the oblique pipe–soil interaction event than the MC model.

3.1 Introduction

Ground displacements—for example, landslides, fault movements and lateral spreading due to soil liquefaction— are some of the most dangerous geohazards that can impose a significant threat to buried pipelines. Ensuring safe and reliable operation of pipelines in the presence of these geohazards is therefore a prime concern for pipeline operators and regulatory agencies.

In current engineering practice, the modes of relative displacement between pipe and soil are generally categorized through three orthogonal springs in lateral, axial and vertical directions. In other words, the stiffness of the soil in three directions is independent of each other and therefore, the deformation in one direction has no effect on the others. However, the loading to the pipeline is not always aligned along one principal direction, and in most of the cases, combined (oblique) loading conditions are expected (Guo 2005; Cocchetti et al. 2009; Daiyan et al. 2011a). An oblique loading can be resulted from the combination of different directional loading, e.g. lateral-vertical, lateral-axial or axial-vertical loading. The response of pipelines buried in dense sands and are subjected to oblique loading in the lateral-vertical direction is the focus of the present study.

Buried pipelines are generally installed into a trench. When the trench is backfilled with sand, the backfill material is generally in a loose to medium dense state. However, during the lifetime of a pipeline, the backfill sand might be densified due to traffic loads, nearby machine vibrations or seismic wave propagation (Kouretzis et al. 2013).

Several experimental (Audibert and Nyman 1978; Hsu 1996; Calvetti et al. 2004; di Prisco and Galli 2006; Merifield et al. 2008), theoretical (Nyman 1982; Cocchetti et al. 2009) and numerical (Calvetti et al. 2004; Yimsiri et al. 2004; Guo 2005; Pike and Kenny 2011; Daiyan et al. 2011a,

2011b; Farhadi Hikooei 2013; Jung et al. 2016) studies were conducted in the past to investigate the pipe–soil interaction in soil during an oblique movement. Very few studies among these were conducted in dense sand. For example, Nyman (1982) proposed an analytical approach, whereas Cocchetti et al. (2009) used FE analysis to calculate the peak oblique soil resistance in dense sand. However, they did not consider the post-peak softening behavior of dense sand. In general, these studies showed the significance of considering the coupling between the loads in different directions on buried pipelines.

Physical tests are generally expensive and in most cases, it is not possible to conduct physical tests for a wide range of parameters. Numerical analysis has, therefore, gained significant attraction in recent years to analyze the complex pipe–soil interaction. One of the main challenges of the numerical modeling of pipe–soil interaction is to choose an appropriate soil constitutive model. For example, although physical tests (Zhang et al. 2002; di Prisco and Galli 2006; Hsu et al. 2006) on oblique pipe–soil interaction in dense sand show post-peak softening behavior, most of the previous numerical studies used the Mohr–Coulomb (MC) model that considers constant friction and dilation angles (Yimsiri et al. 2004; di Prisco and Galli 2006; Jung et al. 2016). The classical MC model cannot capture the post-peak softening behavior of dense sand (Guo 2000; Roy et al. 2016). Furthermore, while using the MC model, in addition to the friction angle, the dilation angle also plays a significant role on lateral or uplift soil resistance of a pipeline. For anchor–soil interaction, Merifield and Sloan (2006) showed that, in extreme cases, the consideration of non-dilatant behavior of dense sand (zero dilation angle) gave the ultimate lateral capacity of approximately half of the capacity of a soil model that satisfies the associated flow rule (dilation angle = friction angle). The above-mentioned study clearly shows the importance of the soil model in numerical modeling of pipe–soil interaction.

In the current design guidelines (e.g. ALA 2005, PRCI 2009) force–displacement relationships during pipe–soil interaction are defined by bilinear or hyperbolic functions. Therefore, the current

guidelines fail to appropriately represent two important practical situations: (i) the post-peak degradation of the soil resistance to pipelines buried in dense sand, and (ii) the oblique loading conditions of the pipelines. The main objective of the present study is to present oblique (lateral-vertical) pipe–soil interaction modeling using an advanced soil model, named the modified Mohr–Coulomb (MMC) model, that can capture the post-peak degradation of soil resistance. A range of oblique loading angles (0 to 90°) is considered for a 300-mm diameter pipe embedded at 900 mm from the ground, surface to the centre of the pipe. The failure mechanisms of soil, i.e., the formation of shearing planes, are investigated to explain possible mechanisms involved in the force–displacement response.

3.2 Finite Element Formulation

Two-dimensional FE analyses in plane strain condition are conducted to model the oblique (lateral-vertical) pipe–soil interaction. The pipe is modelled as a rigid body. Four-node, bilinear plane strain, reduced integration with an hourglass control element (CPE4R in Abaqus) is used for modelling the soil. The structured mesh is generated in Abaqus/CAE by zoning the soil domain. Figure 3.1 shows the typical FE mesh used in the present study. The soil is defined as an adaptive mesh domain with default Lagrangian type boundary regions, which results in new smooth mesh with improved aspect ratios at a given interval.

The vertical faces of the soil domain are restrained from any lateral movement by using roller supports and the bottom face is restrained from the vertical and horizontal movement using hinge supports. No displacement boundary condition is applied at the top surface of the domain so that soil can move freely in the upward direction. The oblique angle (α) is defined as the angle of loading direction with the vertical, as shown in Fig. 3.1. The pipe is pulled in the oblique direction by defining both upward and lateral displacements during the loading step. For example, ~87 mm and ~50 mm

displacements in the horizontal and vertical directions, respectively, are applied to the pipe centre to displace the pipe ~100 mm at an angle of 60° with the vertical.

To keep the pipe in the "wished-in-place" configuration, the centre of the pipe is placed at a distance H from the ground surface. The depth of the pipe is measured in terms of $\widetilde{H}$ (= H/D), which is termed the "embedment ratio." The size of the soil domain is kept sufficiently large so that no boundary effects on the oblique resistance and soil failure mechanism are expected.

The interaction between pipe and soil is modeled using the contact surface approach available in Abaqus/Explicit. The Coulomb friction model is used, where the friction coefficient (μ) is defined by $\mu = \tan(\phi_\mu)$, ϕ_μ being the interface friction angle.

The authors are aware that the installation of the pipe may cause some disturbance to the soil closer to the pipe. However, the effect of such disturbance is not considered in the present study.

3.3 Modelling of soil

Two soil constitutive models, the Mohr–Coulomb (MC) and a modified Mohr–Coulomb (MMC), are used in the present study. In the classical MC model, constant values of angles of internal friction (ϕ') and dilation (ψ) are defined. However, the MMC model proposed by Roy et al. (2016) considers the effects of pre-peak hardening, post-peak softening, density and confining pressure on mobilized angles of internal friction (ϕ') and dilation (ψ) of dense sand.

A detailed discussion of the MMC model, estimation of model parameters and comparison with the MC models are available in Roy et al. (2016, 2018a) and is not repeated here. However, the constitutive equations are summarized in Table 3.1. The soil parameters used in the present FE analysis are shown in Table 3.2. Note that the mesh size influences FE simulation results when softening behavior of the soil is considered. However, this issue has not been discussed in the present study.

3.4 Results

The FE model was first validated for two 1g model tests with 100-mm diameter pipe for pure lateral ($\widetilde{H}$ = 5.5) and pure vertical loading ($\widetilde{H}$ = 3) conditions, conducted by Trautmann (1983) and Cheuk et al. (2005, 2008), respectively. These tests were conducted in dense sand, having $D_r \sim 80\%$ for lateral loading (Trautmann 1983) and 92% for upward loading (Cheuk et al. 2005, 2008), respectively. Details of the validation of the FE model and performance of the MMC model can be found in Roy et al. (2016, 2018b) and are not repeated here due to the space limitation. For the present study, a 300-mm diameter pipe buried at $\widetilde{H}$=3 was pulled at different oblique angles (α) ranging from 0 to 90°, as shown in Fig. 3.1. The force–displacement behavior and the associated failure mechanism are discussed in the following sections. In the following sections, unless noted otherwise, the force–displacement curves are presented in normalized forms as N_o ($=F_o/\gamma HD$) versus w/D, where F_o is the oblique resistance on the pipe per unit length (Fig. 3.1); H is the depth of the center of the pipe from the soil surface prior to pulling, γ is the dry unit weight of soil, and w is the oblique displacement. The peak value of N_o is defined as N_{op}, and the displacement required to reach to the peak is defined as w_p.

3.5 Force–Displacement Behaviour

Figure 3.2 shows the normalized force–displacement curves for α = 0 to 90°. For α = 0 - 60°, N_o increases with w/D, reaches the peak (N_{op}) and then gradually decreases with w/D, which is primarily due to the strain-softening behaviour of dense sand. After a certain w/D, N_o becomes almost constant. However, for α = 75 - 90°, N_o increases with w/D, reaches point A, creating a plateau shape and then increases again with w/D (Fig. 3.2). Note that for a certain α, the pipe was pulled out in the oblique direction, defining both horizontal and vertical displacements at the pipe reference point, as shown in Fig. 3.1. For example, for α = 90°, the pipe is displaced by defining the horizontal displacement

while keeping the vertical displacement as zero. As the pipe cannot move upward, after reaching point A (Fig. 3.2), instead of decreasing, N_o starts to increase again with w/D. A similar reason governs the force–displacement behaviour for $\alpha = 75°$, no post-peak softening after the peak. For further clarification, an additional FE analysis for $\alpha = 90°$ has been conducted by applying a horizontal displacement at the pipe centre, however, the pipe is free to move in the vertical direction. The force–displacement behaviour obtained from this analysis is also plotted in Fig. 3.2 (broken line). A clear post-peak softening behaviour of the force–displacement curve after the peak is evident when the pipe is free to move in the vertical direction. Although most of the available physical test results on pure lateral loading (Trautmann 1983, Wijewickreme 2009) show a clear post-peak softening behaviour of the force–displacement curve, due to the ability of pipe to move vertically, the continuous increase of the force–displacement curve (i.e., no post-peak degradation), when the pipe was restrained vertically, was also obtained by Fenza (2016) in their physical test results on 219.1-mm diameter pipe buried in sand and pulled at $\alpha = 90°$. Figure 3.2 also shows that the peak oblique resistance (N_{op}) is maximum for $\alpha = 90°$ and minimum for $\alpha = 0$. Similar results were also found by Daiyan et al. (2011b) for their oblique pipe loading tests in dense sand.

To show the advantages of the MMC model, three FE simulations with the MC model were also conducted for $\alpha = 60°$ using three sets of ϕ' and ψ values $\phi' = 45°, \psi = 17°$; $\phi' = 45°$, $\psi = 0°$ and $\phi' = 35°$, $\psi = 0°$).

For the MC model, N_o increases with w/D, reaches a peak (N_{op}) and then remains almost constant (Fig. 3.3). As shown in Fig. 3.3, the dilation angle plays a significant role in the oblique resistance of pipeline. For the MC model with $\phi' = 45°, \psi = 17°$, N_{op} is significantly higher compared to $\phi' = 45°, \psi = 0°$. Furthermore, the peak oblique resistance with the MC model for $\phi' = 45°, \psi = 17°$ is ~33%

higher than the peak oblique resistance obtained from the MMC model. Another key observation from Fig. 3.3 is that the simulations with the MC model do not show any post-peak degradation of N_o, as observed in the physical tests and FE simulations with the MMC model.

FE analyses are also conducted with the three sets of the MC model for a wide range of α (= 0 - 90°) and the peak oblique resistance is plotted against α in Fig. 3.4. The peak oblique resistance obtained from the FE analysis with the MMC model is also plotted in Fig. 3.4 for further comparison. For the MC model, the difference in the peak oblique resistance for three sets of ϕ' and ψ values is higher for α = 90° and the difference gradually decreases as α decreases (Fig. 3.4). In other words, the representative values of ϕ' and ψ also depend on α. For example, although ϕ' = 44° and ψ = 16° gives N_{op} comparable to N_{op} obtained from the MMC model for α = 30°, the same mobilized values of ϕ' = 44° and ψ = 16° do not necessarily give comparable N_{op} for α = 75°. Therefore, one must be extremely careful in choosing the representative values of ϕ' and ψ when using the MC model to calculate the oblique resistance. However, the MMC model does not require the representative values of ϕ' and ψ to be defined; rather, the MMC model requires ϕ'_c value, which can be easily obtained from typical laboratory tests.

Figure 3.5 shows the dimensionless horizontal vs vertical components of the reaction force for α = 0 - 90° for both the MC and MMC models. For a certain α, the peak oblique resistance as well as the horizontal and vertical components of the oblique resistance can be calculated from Fig. 3.5. As mentioned earlier, the current design guidelines (e.g. ALA 2005 and PRCI 2009) consider only the pure peak lateral and vertical resistances and therefore, may not necessarily represent the oblique pipe–soil interaction events. The peak lateral and uplift resistances calculated from PRCI 2009 and ALA 2005 are also plotted in Fig. 3.5, for representative friction angle of dense sand. Figure 3.5

shows that one needs to be extremely careful in choosing the representative value of the friction angle for calculating the peak lateral and uplift resistances. Furthermore, the present study extends the result to oblique resistances for a wide range of α that the current design guideline does not explicitly represent.

3.6 Failure Mechanisms

The difference in the oblique resistance for different oblique angles (α) with the MMC model can be explained by the progressive development of shear bands. The plastic shear strains developed in soil at an oblique displacement of 50 mm (w/D = 0.17) for α = 60° with the MMC model are shown in Fig. 3.6. As shown, significantly large plastic shear strains develop in some narrow zones at this level of oblique displacement. Three distinct shear bands, f_1, f_2 and f_3 are formed, as shown in Fig. 3.6. The shear bands in Fig. 3.6 are very similar to the model tests of Turner (2004) for lateral pipe–soil interaction in dense sand. In the MMC model, ϕ' and ψ are not constant but vary with plastic shear strain. The strain localization initiates at high values of ϕ' and ψ near the peak which eventually reduces to the critical state at moderate to large displacements. As the post-peak softening of stress–strain behavior is not considered, the MC model cannot simulate the degradation of N_o after the peak, as shown in Fig. 3.3.

Broken lines through the highly concentrated γ^p zone (Fig. 3.6) are drawn for further investigation of the location of the shear bands for different α. As in Fig. 3.6, the locations of the shear bands are also obtained for α = 45° and plotted in Fig. 3.7 for w/D=0.17. Figure 3.7 shows that the inclination of the shear band with the horizontal decreases with an increase in α, which results in higher resistance for higher α.

The size of the failure wedge for $\alpha = 60°$ is higher than that of $\alpha = 45°$ and therefore, the oblique resistance is higher for $\alpha = 60°$. For a similar reason, $\alpha = 0°$ results in the lowest resistance whereas $\alpha = 90°$ results in highest resistance. However, the oblique resistance is a function of not only the size of the failure wedge but also the mobilized ϕ' and ψ values along the shear band. The MMC model can successfully capture both features of the oblique pipe–soil interaction.

3.7 Conclusions

Finite element analysis of oblique pipe–soil interaction (lateral–vertical) is conducted for a 300-mm diameter pipe buried at 750 mm (from the ground surface to the center of pipe) for a wide range of oblique angles ranging from 0° to 90°. The analyses are conducted using Abaqus/Explicit FE software. Recognizing the fact that the constitutive model of sand influences the calculated resistance, a comparative study is performed using the built-in Mohr–Coulomb model in Abaqus and a modified Mohr–Coulomb (MMC) model. The progressive formation of shear bands and their relation to the force–displacement response is carefully examined. Results show that the MMC model can better simulate the oblique pipe–soil interaction event than the built-in MC model. The analysis presented in the paper is only for one geometry and set of soil properties. Further study of the effects of depth of embedment, pipe diameter and soil parameters is required.

3.8 Acknowledgements

The work presented in this paper has been supported by the Natural Sciences and Engineering Research Council of Canada (NSERC), Petroleum Research Newfoundland & Labrador and Mitacs.

3.9 References

American Lifelines Alliance (ALA) 2005. *Guidelines for the Design of Buried Steel Pipe*. <https://www. americanlifelinesalliance.com/pdf/Update061305.pdf > (Mar. 13, 2018).

Audibert, J.M. and Nyman, K.J. 1977. Soil restraint against horizontal motion of pipes. *ASCE Journal of Geotechnical Engineering Division*, 103(10): 1119–1142.

Calvetti, F., di Prisco, C. and Nova, R., 2004. Experimental and numerical analysis of soil–pipe interaction. *Journal of Geotechnical and Geoenvironmental Engineering*, 130(12): 1292–1299.

Cheuk, C. Y., White, D. J. and Bolton, M. D. 2005. Deformation mechanisms during the uplift of buried pipelines in sand. *Proc., 16th International Conference on Soil Mechanics and Geotechnical Engineering*, Osaka, 1685–1688.

Cheuk, C. Y., White, D. J. and Bolton, M. D. 2008. Uplift Mechanisms of Pipes Buried in Sand. *Journal of Geotechnical and Geoenvironmental Engineering*, 134(2): 154–163.

Cocchetti, G., di Prisco, C., Galli, A., & Nova, R. 2009. Soil–pipeline interaction along unstable slopes: a coupled three-dimensional approach. Part 1: Theoretical formulation. *Canadian Geotechnical Journal*, 46(11): 1289–1304.

Daiyan, N., Kenny, S., Phillips, R. and Popescu, R. 2011a. Investigating pipeline–soil interaction under axial–lateral relative movements in sand. *Canadian Geotechnical Journal*, 48(11): 1683–1695.

Daiyan, N., Kenny, S., Phillips, R. and Popescu, R. 2011b. Numerical investigation of axial-vertical and lateral-vertical pipeline/soil interaction in sand. *14th Pan-American Conference on Soil Mechanics and Geotechnical Engineering.* Toronto, Ontario, Canada.

Farhadi H. B. 2013. Numerical modeling of pipe-soil interaction under transverse direction. Ph.D. Thesis, University of Calgary.

Fenza, G. 2016. Experimental and numerical investigations to assess the behaviour of a buried pipeline in areas with high geological instability. Ph.D. Thesis, University of Calgary.

Guo, P. 2000. Modelling granular materials with respect to stress-dilatancy and fabric: A fundamental approach. Ph.D. Thesis, University of Calgary.

Guo, P. 2005. Numerical modeling of pipe–soil interaction under oblique loading. *Journal of Geotechnical and Geoenvironmental Engineering*, 131(2): 260–268.

Hsu, T.W. 1996. Soil restraint against oblique motion of pipelines in sand. *Canadian Geotechnical Journal*, 33(1): 180–188.

Hsu, T.W., Chen, Y.J. and Hung, W.C. 2006. Soil restraint to oblique movement of buried pipes in dense sand. *Journal of Transportation Engineering*, 132(2): 175–181.

Jung, J.K., O'Rourke, T.D. and Argyrou, C. 2016. Multi-directional force–displacement response of underground pipe in sand. *Canadian Geotechnical Journal*, 53(11): 1763–1781.

Kouretzis, G.P., Sheng, D. and Sloan, S.W. 2013. Sand–pipeline–trench lateral interaction effects for shallow buried pipelines. *Computers and Geotechnics*, 54: 53–59.

Merifield, R.S. and Sloan, S.W. 2006. The ultimate pullout capacity of anchors in frictional soils. *Canadian Geotechnical Journal*, 43(8): 852–868.

Merifield, R., White, D.J. and Randolph, M.F. 2008. The ultimate undrained resistance of partially embedded pipelines. *Géotechnique*, 58(6): 461–470.

Nyman, K.J., 1982. Soil response against the horizontal-vertical motion of pipes. *American Society of Civil Engineers*.

Pike, K. and Kenny, S. 2011. Advancement of CEL procedures to analyze large deformation. *Offshore Technology Conference*, 2-5 May, Houston, Texas, USA, doi.org/10.4043/22004-MS.

PRCI (2009). Guidelines for constructing natural gas and liquid hydrocarbon pipelines through areas prone to landslide and subsidence hazards. Pipeline Research Council International.

Roy, K., Hawlader, B.C., Kenny, S. and Moore, I. 2016. Finite Element Modeling of Lateral Pipeline−Soil Interactions in Dense Sand, *Canadian Geotechnical Journal*, 53(3): 490–504.

Roy, K., Hawlader, B.C., Kenny, S. and Moore, I. 2018a. Upward pipe–soil interaction for shallowly buried pipelines in dense sand, *Journal of Geotechnical and Geoenvironmental Engineering*, ASCE, 144(11): 04018078.

Roy, K., Hawlader, B.C., Kenny, S. and Moore, I. 2018b. Lateral resistance of pipes and strip anchors buried in dense sand. *Canadian Geotechnical Journal* (In press, published online on March 22, 2018)

Trautmann, C. 1983. Behavior of pipe in dry sand under lateral and uplift loading. Ph.D. thesis, Cornell University, Ithaca, NY.

Turner, J.E. 2004. Lateral force–displacement behavior of pipes in partially saturated sand. M.Sc. Thesis, Cornell University, Ithaca, NY.

Wijewickreme, D., Karimian, H. and Honegger, D. 2009. Response of buried steel pipelines subjected to relative axial soil movement. *Canadian Geotechnical Journal*, 46(7): 735–752.

Yimsiri, S., Soga, K., Yoshizaki, K., Dasari, G.R. and O'Rourke, T.D. 2004. Lateral and upward soil–pipeline interactions in sand for deep embedment conditions. *Journal of Geotechnical and Geoenvironmental Engineering*, 130(8): 830–842.

Zhang, J., Stewart, D.P. and Randolph, M.F. 2002. Modeling of shallowly embedded offshore pipelines in calcareous sand. *Journal of Geotechnical and Geoenvironmental Engineering*, 128(5): 363–371.

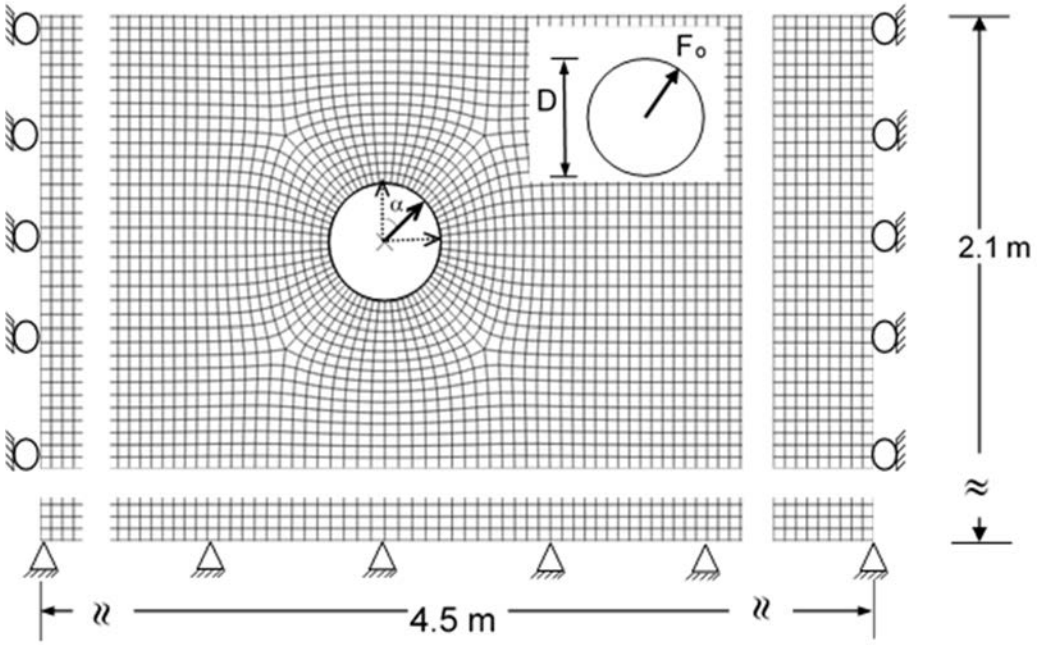

Figure 3.1 Typical finite element mesh for $\widetilde{H}$ = 3 and D =300 mm

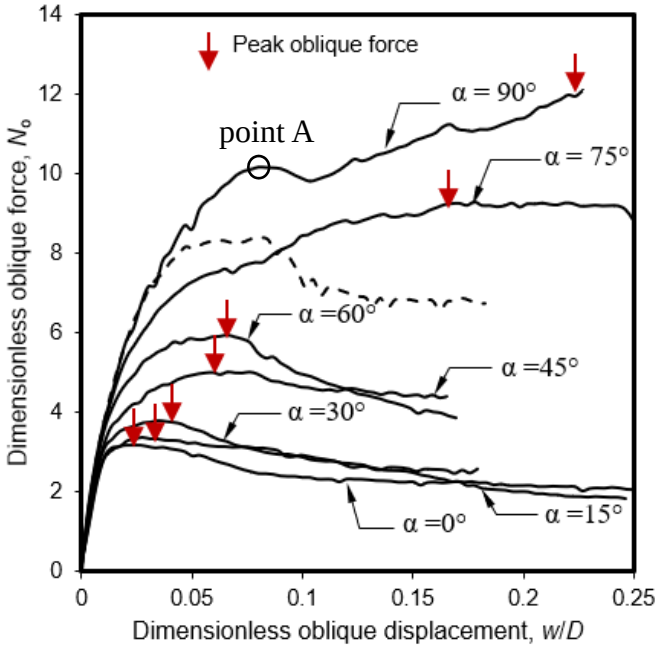

Figure 3.2 Dimensionless force vs displacement plot for different oblique angles

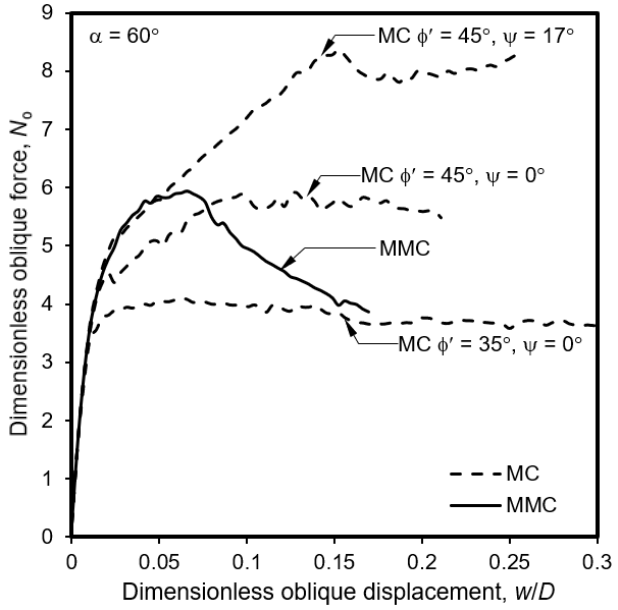

Figure 3.3 Dimensionless force vs displacement plot for both MC and MMC model

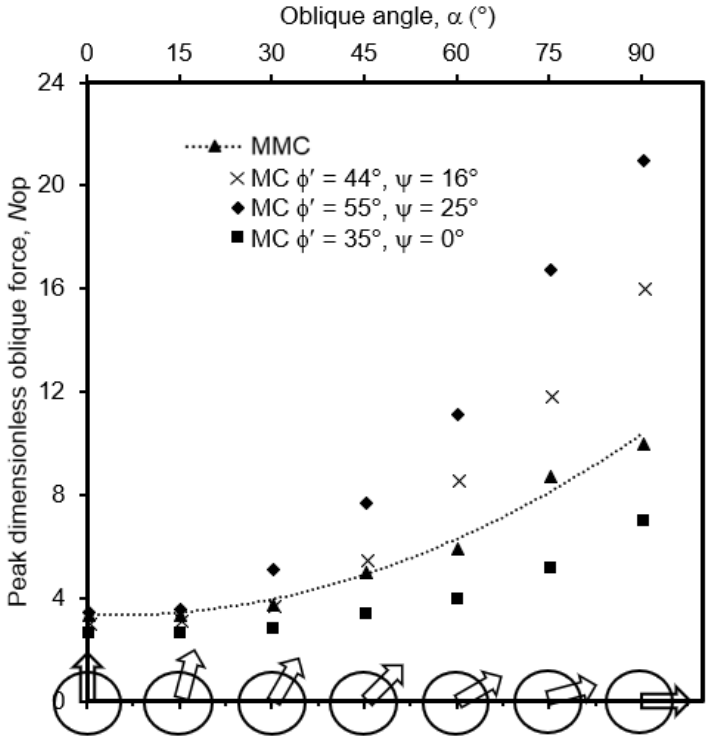

Figure 3.4 Peak dimensionless oblique force vs oblique angle for both MC and MMC models

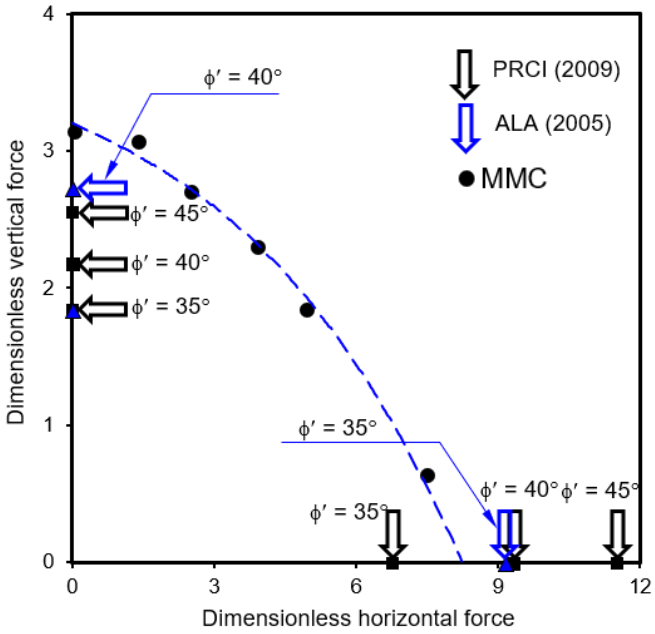

Figure 3.5 Dimensionless vertical force vs dimensionless horizontal force (MMC model)

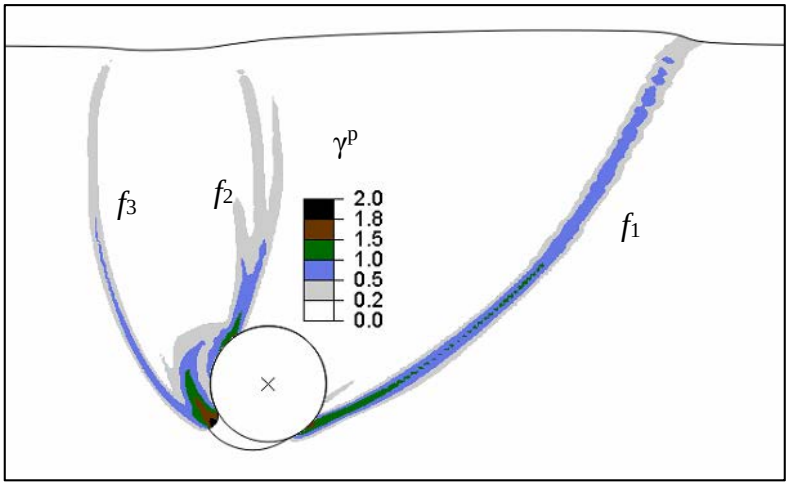

Figure 3.6 Formation of the shear band for the MMC model (α = 60°, w/D = 0.17)

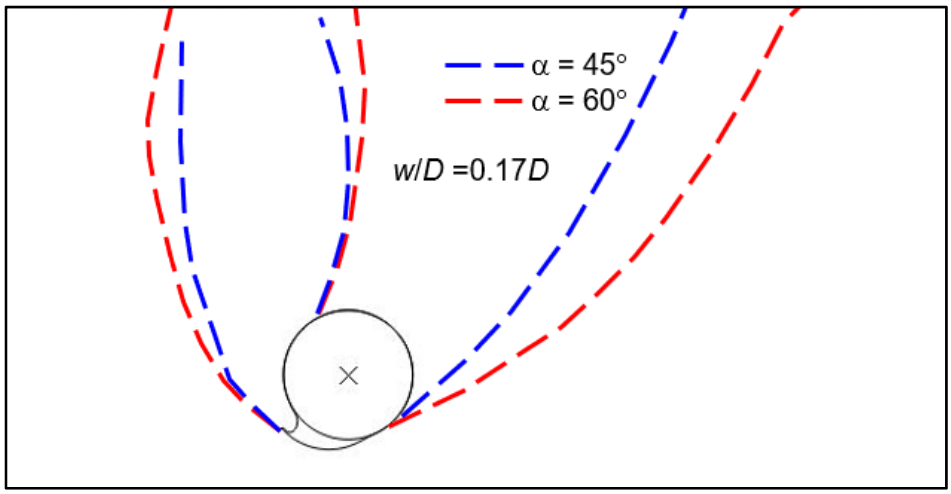

Figure 3.7 Formation of shear bands for the MMC model for α = 45° and 60°

Table 3.1 Equations for Modified Mohr–Coulomb Model (MMC) (summarized from Roy et al. 2016)

Description	Eq. #	Constitutive Equations
Relative density index	(1)	$I_R = I_D(Q - \ln p') - R$, where $I_D = D_r(\%)/100$
Peak friction angle	(2)	$\phi'_p - \phi'_c = A_\psi I_R$
Peak dilation angle	(3)	$\psi_p = \frac{\phi'_p - \phi'_c}{k_\psi}$
Strain softening parameter	(4)	$\gamma_c^p = C_1 - C_2 I_D$
Plastic shear strain at ϕ'_p	(5)	$\gamma_p^p = \gamma_c^p \left(\frac{p'}{p'_a}\right)^m$
Mobilized friction angle at Zone–II	(6)	$\phi' = \phi'_{in} + \sin^{-1}\left[\left(\frac{2\sqrt{\gamma^p \gamma_p^p}}{\gamma^p + \gamma_p^p}\right)\sin(\phi'_p - \phi'_{in})\right]$
Mobilized dilation Angle at Zone–II	(7)	$\psi = \sin^{-1}\left[\left(\frac{2\sqrt{\gamma^p \gamma_p^p}}{\gamma^p + \gamma_p^p}\right)\sin(\psi_p)\right]$
Mobilized friction angle at Zone–III	(8)	$\phi' = \phi'_c + \left(\phi'_p - \phi'_c\right)\exp\left[-\left(\frac{\gamma^p - \gamma_p^p}{\gamma_c^p}\right)^2\right]$
Mobilized dilation angle at Zone–III	(9)	$\psi = \psi_p \exp\left[-\left(\frac{\gamma^p - \gamma_p^p}{\gamma_c^p}\right)^2\right]$
Young's modulus	(10)	$E = K p_a' \left(\frac{p'}{p_a'}\right)^n$

Table 3.2 Parameters used in FE analyses

Parameters	Value
Pipe diameter, D (m)	0.3
K	150
n	0.5
Atmospheric pressure, p'_a (kN/m^2)	100
ν_{soil}	0.2
A_ψ	5
k_ψ	0.8
Initial angle of internal friction, ϕ'_{in} (°)	29
C_1	0.22
C_2	0.11
m	0.25
Critical state of friction angle, ϕ'_c (°)	35
Relative density, D_r (%)	80
Dry unit weight γ (kN/m^3)	17.7
Interface friction coefficient, μ	0.32
Embedment ratio, H/D	3
Cohesion, c' (kN/m^2)	0.1[1]

[1]A very small cohesion value is used to avoid the numerical issue although $c' = 0$ for sand.

Chapter 4
Modeling of Buried Pipelines in Dense Sand under Oblique Motion in Vertical–Horizontal Plane

Co-Authorship: This chapter has been prepared to submit to a journal as a technical paper for review as: Morshed, M. A., Roy, K. and Hawlader, B. C. (2019), "Modeling of Buried Pipelines in Dense Sand under Oblique Motion in Vertical–Horizontal Plane." Most of the research in this chapter has been conducted by the first author. He also prepared the draft manuscript. The other authors mainly supervised the research and reviewed the manuscript.

Abstract:

Finite element modeling of pipelines buried in dense sand under oblique loading in vertical (upward)–horizontal load space is presented. The pre-peak hardening, post-peak softening, density and confining pressure dependent behavior of sand are considered in the simulations for monotonic oblique displacements of the pipeline. The plots of vertical and horizontal components of oblique force (load paths) show a significant non-associated response for shallow burial depths and lateral loading. The restraint to vertical displacement during lateral loading increases the lateral resistance. A simplified approach based on maximum vertical and lateral restraints, together with an inclination factor, is proposed to estimate the maximum oblique resistance.

Author keywords: Pipeline; Mohr-Coulomb model; Finite-element analyses; Dense sand; Oblique loading; Shear bands; Failure mechanisms.

4.1 Introduction

Buried pipelines are commonly used to transport oil and gas over a large distance through a wide variety of soils in varying geological formations and geographical features. One of the major

challenges in the route selection and design is the assessment of geohazard and ground movement effects on pipelines. Many pipeline damage/failures have been reported to be caused by slope failures and ground movements (Baum et al. 2008; Girgin and Krausmann 2015; EGIG, 2018). When a slope fails, the relative movement between the pipeline and surrounding soil might occur in the pure axial, lateral (horizontal) and vertical (uplift and bearing) directions, or also at an oblique angle in the axial–lateral, axial–vertical and vertical–lateral planes. The behavior of pipelines buried in dense sand under oblique loading in the vertical (upward)–horizontal load space is investigated in this study.

The soil restraint due to the relative movement between the pipeline and soil depends on several factors, including the geotechnical properties and constitutive behavior of soil, the direction of load and displacement of the pipe, and soil failure mechanisms (i.e., development of failure wedges and plastic shear zones). A large number of previous studies focused on pure axial, lateral, uplift and penetration resistances (Trautmann 1983; Cheuk et al. 2008; Wijewickreme et al. 2009; Kouretzis et al. 2014; Burnett 2015; Robert and Thusyanthan 2015). In physical modeling, a pipe section is pulled along these directions by applying a given rate of displacement at the end of a flexible loading system (e.g. wire or cable) and the corresponding applied force is measured (Hsu 1996; Calvetti 2004; Monroy et al. 2015). The pipe might move in the other directions during loading; for example, a vertical displacement (v) of the pipe was observed during the unrestrained lateral loading ($v \neq 0$) (Trautmann 1983). Tests were also conducted for restrained lateral loading ($v = 0$) (Zhang et al. 2002; Fenza 2016), and a higher lateral soil restraint was found for restrained cases than that of unrestrained loading (Fenza 2016). Most of the numerical analyses available in the literature have been conducted for unrestrained lateral loading (Jung et al. 2013; Roy et al. 2016). The design guidelines for estimating soil spring constants do not mention the effects of restrained/unrestrained conditions explicitly (ALA 2005; PRCI 2017).

Similar to the physical experiments for lateral loading, a pipe section is pulled at an oblique angle using a flexible loading system in oblique loading tests (Hsu 2006; Wijewickreme et al. 2017). However, in the numerical analysis using finite element (FE) and distinct element methods, a rigid pipe section is pulled at an oblique angle (fixed displacement path) (Calvetti et al. 2004; di Prisco and Galli 2006; Cocchetti et al. 2009). Physical and numerical studies also show that the direction of resultant load and displacement does not coincide in oblique loading cases (Cocchetti et al. 2009); therefore, a non-associated flow rule needs to be considered for modeling the force–displacement response (Zhang et al. 2002).

An elastic–perfectly plastic soil model based on the Mohr–Coulomb (MC) failure criteria is commonly used in FE analyses of pipe–soil interaction, where the soil properties are defined using the "equivalent" angle of internal friction and dilation. However, experimental evidence shows that the mobilized value of these two shear strength parameters depends on confining pressure, relative density of sand and accumulated plastic shear strains, especially for dense sand (Ahmed 1973; Bolton 1986; Turner and Kulhawy 1987). Some of the previous studies considered these factors in the FE analysis for uplift and lateral loading (Jung et al. 2013; Robert 2017; Roy et al. 2016, 2018b).

To calculate the maximum oblique load (F_{op}), simplified expressions have also been proposed, generally in the form of an interaction diagram (yield envelope), as a function of an inclination factor and the maximum lateral and uplift resistances, and also penetration resistances in some cases (Nyman 1984; Hsu et al. 1996; Calvetti et al. 2004; Cocchetti et al. 2009). The behavior is purely elastic inside the yield envelope. However, numerical analyses for pure vertical uplift and lateral loading show the development of plastic strains in the soil before the mobilization of F_{op} (Jung et al. 2013; Roy et al. 2018a, b). The concept of bounding surface (Dafalias and Herrmann 1982) has been used to consider the gradual transition from elastic to plastic behavior inside the bounding surface (Zhang et al. 2002).

This study aims to present FE modeling of the oblique pipeline–soil interaction in the vertical (uplift)–horizontal plane. A modified form of the Mohr–Coulomb model for dense sand is used to simulate the progressive formation of failure planes during loading. The role of restrained and unrestrained loading conditions in constructing the bounding surface is discussed. The influence of shear bands (zones of localized plastic shear strain) on the non-associated behavior in oblique loading is examined. Finally, a simplified approach is proposed to estimate the maximum oblique resistance.

4.2 Problem Statement and FE Modeling

Two-dimensional FE analyses in plain strain condition are performed using Abaqus/Explicit FE software (Dassault Systèmes 2010). A pipe section of diameter D at the burial depth H (i.e., embedment ratio, $\widetilde{H}$ (= H/D)) is pulled at an oblique angle with the vertical (α) (Fig. 4.1). Analyses are performed for D = 200 mm and 500 mm, and $\widetilde{H}$ = 2–10. The effects of installation, for example, the variation of geotechnical properties in the backfill material and native soil, are not considered.

Figure 4.1 shows the typical FE mesh used in the present study at the start of the oblique loading. The structured mesh is generated by zoning the soil domain. An adaptive mesh domain with default Lagrangian type boundary regions is used to alleviate mesh distortion issues, which generates a new smooth mesh with improved aspect ratios at a given interval. The pipe is modeled as a rigid body, and the soil is modeled as a four-node bilinear plane strain quadrilateral and reduced integration with hourglass control elements.

The bottom of the domain is restrained from vertical and horizontal movements, and the vertical faces are restrained from horizontal movement. No displacement boundary condition is applied at the ground surface. The left and right boundaries are placed sufficiently far from the pipe (8.0D and 15.5D from the pipe center (Fig. 4.1)) to avoid boundary effects on the force–displacement behavior.

The pipe–soil interface friction coefficient (μ) is defined as $\mu = \tan(\phi_\mu)$, where ϕ_μ is the interface friction angle that depends on pipe surface roughness and the angle of internal friction (ϕ') of the soil. As explained in the later sections, ϕ' does not remain constant during loading. For example, the soil elements around the pipe might experience high plastic shear strains during oblique displacement that could reduce ϕ' from the peak to the critical state value. Assuming a looser soil condition resulting from plastic shear strains, μ = 0.32 is used in the present study. Note that μ does not affect the simulation results significantly (Rowe and Davis 1982; Yimsiri et al. 2004; Roy et al. 2018a).

In FE analysis, the geostatic stress is applied first under K_0 = 1.0, where K_0 is the at-rest earth pressure coefficient. Based on stress measurements in large-scale tests at Cornell University, Jung et al. (2013) suggested that K_0 ~ 1.0 is an appropriate value after pipe installation and compaction. Moreover, their FE analyses show a small change in the peak force (~3%) for K_0 = 0.3 and 1.0. In the second step, the pipe is pulled at an oblique angle (α) by applying an oblique displacement, $w = \sqrt{u^2 + v^2}$, at the pipe center, where u (= $w\sin\alpha$) and v (= $w\cos\alpha$) are the horizontal and vertical components of the oblique displacement, respectively. The horizontal (F_h) and vertical (F_v) components of the reaction force at the reference point (pipe center) are obtained for each time increment and then the oblique force (F_o) is calculated as $F_o = \sqrt{F_h^2 + F_v^2}$. All the forces are expressed per unit length of the pipeline. As the displacement-controlled loading is applied, the pipe always moves at the given α; however, the angle of the resultant force to the vertical upward direction, α^* ($= \tan^{-1}(F_h/F_v)$) may not be always equal to α.

4.3 Modeling of Soil

A modified Mohr–Coulomb (MMC) model proposed by Roy et al. (2016) is used to model the soil behavior. However, some analyses are also performed with the Mohr–Coulomb (MC) model to show the similarities and differences in simulation results using the MC and MMC models. A detailed

discussion of the MMC model, including the selection of model parameters by calibrating against laboratory tests data, implementation in Abaqus FE software using a subroutine, mesh sensitivity, and performance to simulate vertical upward and lateral pipe–soil interactions, has been presented in previous studies (Roy et al. 2016, 2018(a–c)). In the simulation with the MC model, constant values of angles of internal friction ϕ' and dilation (ψ) are defined. The key features of the MMC model are that ϕ' and ψ vary with mean effective stress (p') and plastic shear strain (γ^p) during loading. The mathematical equations for the MMC model are shown in Table 4.1; these capture the effects of pre-peak hardening, post-peak softening, density and confining pressure on mobilized $\phi'$and ψ. All the parameters are defined in Table 4.2.

4.4 Results

4.4.1 Comparison of simulation with MC and MMC models

Fig. 4.2 shows the variation of normalized oblique force ($N_o = F_o/\gamma HD$) with normalized oblique displacement ($\widetilde{w} = w/D$) for the 200-mm diameter pipe buried at $\widetilde{H}$ = 4 and pulled at α = 45°. The simulations are performed with the MC and MMC models. The soil parameters used in the MMC model are listed in Table 4.2. Moreover, Q = 10 and R = 1 are used (Bolton 1986). Further details on the selection of soil parameters, especially the pre-peak hardening and post-peak softening parameters, are available in the work of Roy et al. (2016). For the MMC model, N_o increases with $\widetilde{w}$, reaches the peak (N_o ~ 5.9 at $\widetilde{w}$ ~ 0.06), quickly decreases to a post-peak value (N_o ~ 4.25 at $\widetilde{w}$ ~ 0.18) and then remains almost constant. The MC model cannot consider the variation of ϕ' and ψ as shown in inset-a of Fig. 4.2. Therefore, two FE simulations are performed with the MC model: one with equivalent values less than the peak (ϕ' = 45°, ψ = 13°) and the other with critical state parameters (ϕ' = 35°, ψ = 0°). Note that the critical state ϕ' is 3°–5° higher in plane strain than in triaxial condition (Pradhan et al. 1988; Yoshimine 2005). Although it is not explicitly mentioned in

the design guidelines, the equivalent values of ϕ' and ψ (less than peak but greater than critical state values) should be carefully selected because they vary with plastic shear strains (inset a in Fig. 4.2). Dickin and Leung (1983) showed that the peak friction angle obtained from laboratory tests significantly overestimates the soil restraints. Note that, for other geotechnical problems, for example, shallow foundations in dense sand, an equivalent friction angle has been recommended to incorporate the effects of progressive failure (Loukidis and Salgado 2011).

To check the effects of earth pressure at-rest, a simulation is performed for the MMC model with K_0 = 0.43 while keeping the other parameters same as described above. Fig. 4.2 shows a very small difference between the force–displacement curves for K_0 = 0.43 and 1.0, which is due to the significant change in stresses in the shear bands (see inset-b) during loading, and therefore the shear resistance along the failure planes is not simply governed by the initial K_0-condition. Previous numerical studies also show very small effects of K_0 on the peak soil resistance; however, the computational time increases significantly (Jung et al. 2013; Roy et al. 2016, 2018a).

Figure 4.2 also shows the force–displacement curves obtained with the MC model. As expected, peak N_o is higher for higher ϕ' and ψ. The small decrease in N_o after the peak with the MC model is primarily due to the reduction of cover depth with oblique displacements.

Inset-b in Fig. 4.2 shows the passive failure wedge where the failure planes are drawn through the highly concentrated shear strain zones, as presented later in the “soil failure mechanisms” section. ϕ' and ψ are constant along these failure planes for the MC model, while they vary with γ^p and p' in the MMC model. The oblique force on the pipe depends on the size of the failure wedge and shear resistance along the failure planes. The largest wedge forms in the simulation with the MC model for ϕ' = 45°, ψ = 13°. The calculated $\widetilde{w}$ at the peak force is higher for this case because a larger

displacement is required to mobilize the peak force resulting from a larger wedge as compared to the smaller wedge for $\phi' = 35°$, $\psi = 0°$ (inset b in Fig. 4.2).

In summary, both peak and post-peak degradation of oblique resistance, as observed in physical experiments (e.g., di Prisco and Galli 2006; Wijewickreme et al. 2017) can be simulated using the MMC model. The peak force can be calculated using the MC model; however, appropriate values for equivalent ϕ' and ψ should be carefully selected. All the analyses presented in the following sections are performed with the MMC model.

4.4.2 Force–displacement behavior

A total of 83 FE analyses are conducted to estimate the oblique resistance of pipes of two diameters (D = 200 mm and 500 mm) for embedment ratios $\widetilde{H}$ of 2–10. Most of the analyses are conducted for $\alpha = 0°– 90°$ because the focus of the present study is to investigate the oblique behavior in vertical (upward)–horizontal loading cases. However, to show the complete bounding surface in the vertical–horizontal plane, two analyses are also performed for $\alpha = 135°$ (inclined downward) and $\alpha = 180°$ (vertical downward) for D = 200 mm and $\widetilde{H} = 4$.

Figure 4.3 shows the oblique force–displacement curves for D = 200 mm and $\widetilde{H} = 4$. For $\alpha = 0°–60°$, the oblique force (N_o) increases with oblique displacement ($\widetilde{w}$), reaches the peak at $\widetilde{w} \leq 0.075$, decreases quickly and then remains almost constant at $\widetilde{w} = 0.2–0.5$. The quick reduction of N_o after the peak is primarily due to the reduction of the friction and dilation angles of the soil with the development of plastic shear strain. Note that, if the analysis is continued to include large displacements, N_o will reduce further, especially for a small $\widetilde{H}$ and the loading cases near the vertical, because of the significant effects of the reduction of cover depth with pipe displacement (Wang et al. 2010; Roy et al. 2018a). The post-peak degradation of N_o does not occur for $\alpha = 75°$ and $\alpha = 90°$ (v

= 0) cases (Fig. 4.3). Instead, a small increase in N_o at large displacements ($\tilde{w}$ ~ 0.15–0.5) is found for α = 75° and the increase of N_o at large $\tilde{w}$ is more significant for α = 90°. The mechanism behind this is explained below.

4.5 Restrained and Unrestrained Loading

The pipe–soil interaction has been investigated in previous studies through physical modeling by displacing a pipe section using different pulling systems. Trautmann (1983) pulled the pipe laterally without applying any constraint on vertical movement ($v \neq 0$). Calvetti et al. (2004) pulled the pipe using a flexible wire and pulley system that guaranteed no vertical constraints and forces during lateral loading. However, Zhang et al. (2002) conducted lateral loading tests using geotechnical centrifuge where the pipe is penetrated to a certain depth and then displaced laterally under no vertical movement (v = 0). Fenza (2016) conducted lateral loading tests for both restrained and unrestrained conditions. For oblique loading, Hsu et al. (1996) pulled the pipe at an angle by selecting the horizontal and vertical drive gears that drive a steel chain. The actual horizontal and vertical displacement components were measured using LVDTs. However, the results are presented for the applied loading angle. Wijewickreme et al. (2017) used a coupling system that consists of end clamps at the ends of the pipe and a double-ended hook cable to pull the pipe.

The numerical modeling of oblique pipe–soil interaction is generally conducted by displacement-controlled pulling of a rigid pipe section along the given loading angle (e.g., Calvetti et al. 2004; Guo 2005; di Prisco and Galli 2006). This implies that the pipe is not allowed to any movement other than the loading direction.

The solid lines in Fig. 4.3 shows the results of FE simulations which are performed through displacement-controlled loading. The pipe is moved along the prescribed direction: for example, the pipe is restrained from moving in the vertical direction (v = 0) in α = 90° case. To investigate the

effects of restraint, a simulation is performed for lateral loading where the pipe is pulled horizontally without restraining vertical movement ($v \neq 0$). In this case, the pipe displaces vertically upward with lateral loading, which is discussed further in the later sections. The dashed line in Fig. 4.3 shows the force–displacement curve for this condition. The normalized force (N_o) for this case represents only the lateral force because the vertical component is zero. Moreover, a post-peak degradation of N_o is found for this loading condition. At large displacements (e.g., $\widetilde{w}$ = 0.15–0.5), the normalized force for $v \neq 0$ ($N_o \sim 8$) is approximately half of that for $v = 0$ case ($N_o \sim 13$–16).

Two more simulations are performed without restraining lateral displacement of the pipe for vertical upward ($\alpha = 0°$) and downward ($\alpha = 180°$) movements. No difference between the normalized uplift or penetration resistance is found from the simulations with and without lateral constraints. Therefore, it can be concluded that constraint to the movement of the pipe perpendicular to the applied direction of the movement is significant near the lateral loading cases, which can be explained using the soil failure and formation of shear bands with loading.

Figure 4.4 shows the shear bands at $\widetilde{w} = 0.48D$ during the lateral displacement for restrained ($v = 0$) and unrestrained ($v \neq 0$) conditions. Three shear bands form in each case. As the pipe cannot move vertically in $v = 0$ case, a triangular wedge ABC forms in front of the pipe and then an inclined upward shear band forms from the tip of the triangular wedge. On the other hand, the pipe moves upward with lateral loading for $v \neq 0$, and the inclined upward shear band forms without the formation of a triangular wedge as in the $v = 0$ case. The passive failure wedge forms by the shear bands f_2' and f_3' is larger than that of f_2 and f_3. Therefore, the oblique resistance for $v = 0$ is higher than that of $v \neq 0$. For $v \neq 0$, the reduction of shear strength in the shear bands due to the accumulation of plastic shear strains and the reduction of burial depth (although small in this case) cause the post-peak degradation of soil resistance (dashed line in Fig. 4.3). However, for $v = 0$, instead of post-peak

reduction, the increase in penetrating resistance of the triangular wedge (laterally) increases the lateral force with the displacement of the pipe. Another observation is that the ground heave for $v \neq 0$ is higher than that of $v = 0$. The shapes of the simulated ground heave and failure wedges are similar to that observed in physical experiments (e.g., Turner 2004; Fenza 2016).

4.6 Vertical Displacement of Pipe in Unrestrained Lateral Loading

The vertical displacement of the pipe for $v \neq 0$ condition is not significant until the mobilization of the peak resistance (e.g., $\widetilde{w} \sim 0.07$, dashed line in Fig. 4.3). After that, the pipe displaces upward at an angle (θ) to the horizontal with lateral displacement; for example, $\theta \sim 20°$ in the simulation for $D = 200$ mm and $\widetilde{H} = 4$. The upward movement is primarily due to lower effective stresses and shear resistance of soil above the springline than that of the elements below the springline, which creates shear bands in upward directions resulting in the formation of active and passive failure wedges.

To investigate the effects of burial depth and pipe diameter, ten analyses are performed for varying embedment ratio ($\widetilde{H} = 2–10$) for two pipe diameters ($D = 200$ mm and 500 mm). Fig. 4.5 shows that the vertical displacement of the pipe decreases with an increase in embedment ratio (i.e., θ decreases with $\widetilde{H}$). Moreover, for a given embedment ratio, the larger the pipe diameter the smaller the θ. The difference in effective stresses and strength between the soil elements above and below the springline decreases with an increase in burial depth; therefore, the vertical displacement of the pipe is smaller for larger $\widetilde{H}$, and it is even smaller for larger diameter pipe because of larger burial depth for a given $\widetilde{H}$. At a very large burial depth, there will be no vertical displacement due to lateral loading and the flow-around mechanisms will govern the lateral displacement (θ).

4.7 Effects of Burial depth on Force–displacement Behavior

The solid lines in Fig. 4.6 show the force–displacement curves of a 200-mm diameter pipe for $\widetilde{H} = 2–10$ and $\alpha = 30°$. The peak normalized oblique force (N_{op}) and oblique displacement required to

mobilize the peak force ($\widetilde{w}_p$) increase with embedment ratio. For example, N_{op} = 3.4 and N_{op} = 9.3 mobilize at $\widetilde{w}_p$= 0.034 and $\widetilde{w}_p$= 0.13 for embedment ratio of 2 and 10, respectively. To investigate the effects of pipe diameter, two FE simulation results for a larger pipe diameter (= 500 mm) buried at $\widetilde{H}$ = 2 and 8 are shown in this figure. Fig. 4.6 shows that the larger the pipe diameter the smaller the normalized oblique resistance (e.g., N_{op} = 7.7 and N_{op} = 6.9 for 200-mm and 500-mm diameter, respectively for $\widetilde{H}$ = 8), which is primarily due to the higher mean stress around the larger diameter pipe that reduces the angles of internal friction and dilation (see Table 4.1). At a large displacement (e.g., $\widetilde{w}$ = 0.35), diameter effects on normalized force reduce because of significant plastic shear strain development around the pipe at this stage that reduces the shear strength parameters to the critical state values, $\phi' = \phi'_c$ and ψ = 0 (see the equations for post-peak softening in Table 4.1) for both pipe diameters.

4.8 Load and Displacement Paths

Figure 4.7 shows the load path (N_h–N_v) and displacement path (u–v) in the vertical–horizontal (V–H) loading plane for the 200-mm diameter pipe buried at $\widetilde{H}$ = 4. Except for the three unrestrained simulations, all the simulation are performed by displacement-controlled loading (i.e., applied a prescribed displacement at a given oblique angle). Therefore, the dashed radial lines represent the displacement paths for varying loading angle. In the three unrestraint simulations, the displacement is applied in the vertical and lateral directions, and the pipe is allowed to move in the V–H plane. The pipe does not move laterally for the vertical upward (α = 0°) or downward (α = 180°) unrestrained simulations because of symmetry; therefore, the load path and displacement path are the same for these simulations. For the lateral unrestrained loading (α = 90°), the pipe displaces upward at an angle θ = 23.5° to the horizontal after reaching close to the peak. The arrows in Fig. 4.7 show the applied displacement paths for restrained cases and displacement path after reaching the peak for

unrestrained cases.

Previous studies show that the load–displacement response of shallow foundations or pipelines under combined vertical and lateral loading or oblique loading can be better explained using an interaction diagram (Gottardi and Butterfield 1995; Zhang et al. 2002). The oblique load capacity is generally defined by a yield envelope (Cocchetti et al. 2009). The inset of Fig. 4.7 shows the bounding surface that is drawn through the points of the maximum oblique load (N_{op}). In the present study, similar to the work of Zhang et al. (2002), the term bounding surface (instead of yield envelope) is used because significant plastic deformation occurs during loading before reaching N_{op}.

Fig. 4.7 shows the typical load paths for α = 0°–90°. The load and displacement paths for a given α (solid and dashed lines) coincide at the early stage of displacement. However, for a non-vertical loading ($\alpha \geq 0°$), the load path deviates to the right from the displacement path when it reaches close to the bounding surface. At any point on the load path (e.g., point X for α = 90°), the direction of the resultant force at any instant can be calculated as $\alpha^* = \tan^{-1}(F_h/F_v)$. Except for α = 0° and 180°, α is not equal to α*, which represent a non-associated loading. The non-associated behavior in oblique loading has also been recognized in previous studies (Cocchetti et al. 2009). Fig. 4.7 shows the non-associated behavior even before the maximum oblique load. Note that, based on the concept of bounding surface (Dafalias and Herrmann 1982), Zhang et al. (2002) modeled the plastic deformation within the bounding surface using a non-associated flow rule.

The non-associated behavior after the yield (e.g., load path XY for α = 90° in Fig. 4.7) is further complex. At large displacements ($\widetilde{w} > \widetilde{w}_p$), the shear band formation, its propagation/shifting and generation of new shear bands influence the lateral and vertical components of oblique load and thereby α*. This is discussed further in the soil failure mechanisms section.

4.9 Effects of Pipe Diameter and Burial Depth on Yield Envelope

The solid lines in Fig. 4.8 show the bounding surface for two embedment ratios ($\widetilde{H}$ = 4 and 8) and two pipe diameters (D = 200 mm and 500 mm) under restrained loadings (v = 0) at α = 0°–90°. As shown in Fig. 4.7 that the load paths deviate significantly downward from the corresponding displacement path after reaching the peak oblique force for α = 75° and 90°. The peak oblique load for α = 90° (point X) is below the horizontal axis. However, for the unrestrained lateral loading cases, the load path is along the horizontal axis. A number of design guidelines (e.g., ALA 2005; PRCI 2017) have been developed based on the results of physical and numerical modeling under unrestrained lateral loading. Moreover, the maximum (ultimate) oblique load capacity has been defined as a function of maximum lateral load capacity (Nyman 1984; Cocchetti et al. 2009). Therefore, in order to identify the effects of restrained/unrestrained lateral load capacity, the bounding surfaces are obtained by drawing lines through the maximum oblique load under restrained loading for α = 0°–75° and under unrestrained loading for α = 90° (dashed lines in Fig. 4.8). This gives a slightly larger bounding surface for shallow burial depths (dashed line) than that of restrained loading case (solid lines). This implies that the yield envelope for restrained oblique loading can be reasonably related to the maximum lateral resistance for an unrestrained condition that lies on the horizontal axis, although the loading conditions are different. However, such relation is not be valid for near horizontal loading because the maximum oblique load point is below the horizontal axis.

Fig. 4.8 shows that the size of the bounding surface increases with the embedment ratio. For a given embedment ratio, the normalized maximum oblique force (N_{op}) is smaller for larger pipe diameter, especially for the loading close to the lateral direction.

The maximum lateral force per unit length of a pipeline buried in sand can be calculated using the ALA (2005) and PRCI (2009) guidelines as:

$$F_{hp} = N_{qh}\gamma HD \quad (1)$$

where N_{qh} (= $f(\phi', H/D)$) is a horizontal bearing capacity factor, which is different in ALA (2005) and PRCI (2009). The guidelines do not consider the strain-softening behavior of sand explicitly; instead, an equivalent ϕ'(< 45°), as a function of relative density, is recommended. The calculated F_{hp} using Eq. (1) for $\widetilde{H}$ = 4 is shown on the horizontal axis in Fig. 4.8 for three values of ϕ'. In the present analysis, the decrease in ϕ' from ϕ'_p to ϕ'_c and ψ from ψ_p to 0 due to strain softening is considered; therefore, the estimation of the equivalent friction is not needed. This issue has been discussed further by the authors in Roy et al. (2018).

4.10 Soil Failure Mechanisms

The progressive formation of shear bands in the soil can explain the force–displacement behavior and load path due to the oblique displacement of the pipe. Figure 4.9 shows the differences in the failure mechanisms for three oblique loading cases for D = 200 mm and $\widetilde{H} = 4$ by plotting accumulated plastic shear strain, $\gamma^p = \int_0^t \sqrt{\frac{3}{2}(\dot{\boldsymbol{\epsilon}}_{ij}^p \dot{\boldsymbol{\epsilon}}_{ij}^p dt)}$, where $\dot{\epsilon}_{ij}^p$ is the plastic deviatoric strain rate tensor. A passive failure wedge forms by the shear bands. The oblique soil resistance primarily comes from two sources: (i) component of the weight of the passive soil wedge in the direction of oblique displacement, and (ii) shear resistance along the failure planes. Figs. 4.9 (a–c) show that, at the pre-peak stage, the shear bands generate only near the pipe and do not reach the ground surface for this case. At this stage, the overall plastic shear strain (γ^p) in the shear band is not large enough to mobilize the peak friction and dilation angles (see the equations for pre-peak ϕ' and ψ in Table 4.1); therefore, a smaller oblique resistance than the peak is obtained. When the peak force mobilizes, the length of the shear bands are longer and γ^p along the shear bands is larger than that of the pre-peak stage (compare Figs. 4.9(a–c) and Figs. 4.9(d–f)). Note that γ^p is not same along the entire length of the

shear bands, and the mobilized shear strength is less than the peak shear strength if $\gamma_p \neq \gamma_p^p$. However, the overall shear resistance along the entire length of the shear bands is the maximum at this stage, which gives the peak oblique force. In other words, the peak force should not be calculated simply using the peak friction and dilation angles; instead, a lower (equivalent) value should be used for simplified calculation or in the Mohr–Coulomb model, as discussed in detail for pure uplift and lateral loading cases in Roy et al. (2018a, b). At the post-peak condition, large γ^p generates in the shear bands which reduces the shear strength following the equations for post-peak ϕ' and ψ in Table 4.1. The shear bands reach the ground surface and a clear passive wedge forms which cause ground heave (Figs. 4.9(g–i)).

4.11 Simplified Equations for Peak Oblique Force

Previous studies proposed the methods to calculate the maximum oblique load and mathematical functions for the yield envelope (bounding surface) (Nyman 1984; Zhang et al. 2002; Calvetti et al. 2004; Cocchetti et al. 2009). Following the analogy between strip anchor and pipeline, Nyman (1984) proposed a method to calculate the maximum oblique resistance as a function of oblique angle and the maximum uplift and lateral restraints. Parabolic and power functions have been used to define the complete yield envelope in the *V–H* plane ($0° \leq \alpha \leq 90°$) based on the maximum uplift, lateral and penetration resistances (Zhang et al. 2002; Calvetti et al. 2004; Cocchetti et al. 2009). As the focus of the present study is to model vertical (upward)–lateral oblique loading, an approach similar to the work of Nyman (1984) is used to develop the following simplified equations for the bounding surface which requires three parameters: the maximum lateral (F_{hp}) and vertical (F_{vp}) restraints, and inclination factor (i). Nyman (1984) calculated F_{hp} and F_{vp} based on Audibert and Nyman (1977) and Vesic (1969), respectively. The pipe was displaced under the restrained condition in Audibert and Nyman (1977).

4.11.1 Maximum lateral and vertical restraints

Considerable number of studies have been conducted for proper estimation of F_{hp} and F_{vp}, which include physical modeling (e.g., Trautmann 1983; Cheuk et al. 2008; Wang et al. 2012), numerical analyses (Yimsiri et al. 2004; Roy et al. 2016, 2018a, b) and analytical approach (White et al. 2008). Based on comprehensive FE analysis, authors of the present study showed that the constitutive model of the soil, including the strain-softening behavior of dense sand, affects F_{hp} and F_{vp}. Roy et al. (2018b) proposed the following equations to calculate the maximum lateral resistance for unrestrained loading ($v \neq 0$):

$$N_{hp} = \frac{F_{hp}}{\gamma H D} = N_{hp0} \widetilde{H}^{m_p} f_D \tag{2}$$

Where, N_{hp0} is the values of N_{hp} for a reference diameter of the pipe (D_0); f_D is a size factor (i.e., the effect of diameter) which can be calculated as $f_D = 0.91(1 + D_0/(10D))$, similar to the work of Guo and Stolle (2005); and m_p is a constant. Roy et al. (2018b) also showed that F_{hp} for an anchor is ~10% higher than that of a similar-sized pipe although these two structures have been considered to be analogous (e.g. Nyman 1984). The burial depth effects is negligible after a critical embedment ratio, $\widetilde{H}_c$; therefore, suggested to replace $\widetilde{H}$ with $\widetilde{H}_c$ in Eq. (2) when $\widetilde{H} \geq \widetilde{H}_c$. Moreover, similar to the work of O'Rourke and Liu (2012), the following equation has been used to calculate N_{hp0}.

$$N_{hp0} = \frac{\left(\widetilde{H} + 0.5\right)^2 \tan\left(45° + \frac{\phi'_e}{2}\right)\left(\sin\beta + \mu_1 \cos\beta\right)}{2\widetilde{H}\left(\cos\beta - \mu_1 \sin\beta\right)} \tag{3}$$

where ϕ'_e is the equivalent friction angle, $\mu_1 = \tan\phi'_e$, and $\beta (= 45° - \phi'_e/2)$ is the inclination of an assumed linear slip plane to the horizontal that generates from the bottom of the pipe to form the passive wedge.

For uplift, Roy et al. (2018c) proposed the following equations to calculate the maximum uplift resistance in dense sand.

$$N_{vp} = \frac{F_{vp}}{\gamma HD} = \left\{1 - \left(\frac{\pi}{8\widetilde{H}}\right) + \widetilde{H}\tan\theta\right\} + F_A\widetilde{H} \tag{4}$$

where

$$F_A = \left(\tan\phi'_e - \tan\theta\right)\left[\frac{1+K_0}{2} - \frac{(1-K_0)\cos 2\theta}{2}\right] \tag{5}$$

where K_0 is the coefficient of earth pressure at-rest, and θ is the angle of vertical inclination of the slip plane which is equal to $\psi (< \phi'_e)$.

Using Eqs. (2–5), N_{hp} and N_{vp} are calculated for varying $\widetilde{H}$ (= 2–10) and pipe diameters (= 200 mm and 500 mm) for the following soil parameters: D_0 = 500 mm, K_0 = 0.43, ϕ'_e = 44°, m_p = 0.37, $\widetilde{H}_c$ = 12 and 7.5 for 200-mm and 500-mm pipe, respectively. The details on selection of these parameters are available in Roy et al. 2018(a, c).

4.11.2 Inclination factor

Based on the superposition of limit equilibrium and bearing capacity theory, Meyerhof (1973) suggested that the inclined capacity of an anchor can be calculated as:

$$F_{op} = i\, F_{vp} \tag{6}$$

where i is a non-dimensional inclination factor for a given angle α.

Extending Meyerhof's concept and based on the anchor–pipe analogy, Nyman (1984) proposed the following modified equation for the inclination factor for pipelines:

$$i = 1 + \frac{0.25\alpha}{90° - 0.75\alpha}(i_u - 1) \tag{7}$$

where i_u is the ratio between the maximum horizontal and vertical restraints ($i_u = N_{hp}/N_{vp}$). Hsu (1996) also developed a similar approach who considered the analogous anchor at the center of the

pipe while Nyman considered it on the periphery (see Wijewickreme et al. (2017) for further discussion). Equation (6) has also been used to compare the maximum oblique resistance obtained from physical model tests (Hsu 1996; Wijewickreme et al. 2017) and numerical analyses (Jung et al. 2016).

4.11.3 Calculated oblique resistance based on simplified equations

Using Eqs. (2–5), the maximum lateral (F_{hp}) and vertical (F_{vp}) restraints are calculated, which are then used to calculate the inclination factor i. The inset of Fig. 4.10 shows the variation of i with oblique angle (α) for varying burial depth and pipe diameter. A very small increase in inclination factor is found for an oblique angle up to 30°; however, it increases rapidly at large oblique angles, especially for small burial depth. The higher the $\widetilde{H}$, the lower the i. Moreover, for a given $\widetilde{H}$, the calculated value of i is smaller for the larger pipe (D = 500 mm). The value of i at 90° represents the maximum inclination factor i_u.

Finally, using the value of F_{hp}, F_{vp} and i, the maximum oblique force (F_{op}) is calculated using Eq. (6). The solid lines in Figs. 4.10(a) and 4.10(b) show the calculated normalized resistances for 200-mm and 500-mm pipes, respectively, which match closely with FE calculated values (symbols) at low α. However, the difference between calculated values based on the simplified equations (Eqs. (2–7)) and FE simulations increases after ~30° although the difference is smaller for larger burial depths. Note that at the point of maximum oblique force, the vertical and horizontal force components do not always make an angle α (Fig. 4.7).

As mentioned in previous sections that the vertical movement of the pipeline during lateral loading plays a major role on the maximum lateral load. If the pipe is moved laterally under restrained condition (v = 0), a larger maximum lateral force (component) will be obtained than unrestrained

lateral force (e.g., points A and B on the horizontal axis in Fig. 4.8). The restrained lateral load has also been considered as lateral soil restraint in some studies (Audibert and Nyman 1977).

The oblique force is also calculated using Eqs. (2–7) using F_{hp} from the FE simulation for $\alpha = 90°$ under $v = 0$ case (e.g., point A in Fig. 4.8), instead of Eq. (2) for the unrestrained condition as used above. The calculated i for this condition is higher than that obtained before, as shown in the inset of Fig. 4.10(a) for $\widetilde{H}$=2, as an example. The dashed lines in Figs. 4.10(a) and 4.10(b) show the calculated oblique resistances for this condition which are very close to the FE calculated maximum oblique resistances. In other words, Nyman's interaction factor (Eq. 7) can be used to find the maximum oblique load; however, appropriate values of F_{hp}, specifically the restrained effect on F_{hp}, should be considered. Finally, Figs. 4.10(a) and 4.10(b) provide only the maximum oblique load, as investigated in some studies (Nyman 1984; Wijewickreme et al. 2017), not the yield envelope, because the point of yield is not at angle α (Fig. 4.7).

4.12 Conclusions

Finite element analyses are performed to investigate pipe–soil interaction for oblique loading in the vertical (upward)–lateral loading space. The analyses are conducted by implementing a modified Mohr–Coulomb (MMC) model which considers the effects on relative density, confining pressure and plastic shear strains on mobilized friction and dilation angles. Analyses are also performed with the Mohr–Coulomb (MC) model and it is shown that the MMC model can capture better a number of features including the shear band formation, failure mechanisms and post-peak degradation in oblique resistance. A simplified approach is proposed to estimate the maximum oblique resistance based on the maximum lateral and vertical resistances and an inclination factor. The following conclusions can be drawn from the present study:

1. The direction of resulting oblique force close to its maximum value and at post-peak stage does not coincide with the direction of applied displacement (i.e., non-associate loading). The non-association is higher in the horizontal loading cases and increases with a decrease in burial depth.
2. The load paths after the maximum oblique load are significantly influenced by the formation and propagation of shear bands. For small oblique angles, the load path might reverse approximately along the direction of pipeline displacement; however, a significant vertical upward component of force generates at large oblique angles that moves the load path away from the direction of pipe movement.
3. The restraint to vertical movement during lateral loading increases the lateral resistance. The effects of restraint are more significant for shallow burial depths.
4. Nyman (1984) inclination factor can be used to estimate the maximum oblique force (F_{op}), provided the maximum lateral (F_{hp}) and vertical (F_{vp}) soil restraints are properly selected. F_{hp} based on unrestrained loading (Roy et al. 2018a, b) underestimates F_{op} at large oblique angles; however, the use of F_{hp} from restrained loading can calculate F_{op} better for all oblique angles less than 90°.

4.13 Acknowledgements

The work presented in this paper has been supported by the Natural Sciences and Engineering Research Council of Canada (NSERC), Equinor (formerly Statoil), Petroleum Research Newfoundland and Labrador (PRNL), and Mitacs.

4.14 List of symbols

The following abbreviations and symbols are used in this paper:

A_ψ = slope of $(\phi'_p - \phi'_c)$ vs. I_R curve;

$C1$, C_2 = material constant

D = diameter of pipe;

D_r = relative density;

D_0 = reference diameter;

E = Young's modulus;

F_A = vertical component of the shear force along the slip plane;

F_h = horizontal force component;

F_{hp} = maximum horizontal force;

F_v = vertical force component;

F_{vp} = maximum vertical force;

F_o = oblique force;

F_p = maximum oblique load;

f_D = size factor for normalized resistance;

H = distance from ground surface to pipe center;

$\widetilde{H}$ = embedment ratio (=H/D);

$\widetilde{H}_c$ = critical embedment ratio;

I_R = relative density index;

i = non dimensional inclination factor;

i_u = ratio between the maximum horizontal and vertical restraints;

K_0 = earth pressure coefficient at-rest;

k_ψ = slope of $(\phi'_p - \phi'_c)$ vs. ψ_p curve;

m_p = constant;

N_h = normalized lateral force;

N_{hp} = normalized maximum lateral force;

N_{hp0} = reference peak normalized lateral force;

N_o = normalized oblique force;

N_{op} = normalized maximum oblique force;

N_{qh} = horizontal bearing capacity factor;

N_v = normalized upward force;

N_{vp} = normalized maximum vertical force;

n = an exponent;

p' = mean effective stress;

P_a' = atmospheric pressure (=100 kPa);

Q, R = material constants (Bolton 1986);

u = lateral displacement of pipe;

v = vertical displacement of pipe;

V = vertical loading direction;

w = oblique displacement of pipe;

$\widetilde{w}$ = normalized oblique displacement of pipe (= w/D);

$\widetilde{w}_p$ = normalized oblique displacement required to mobilize N_{op};

α = oblique angle;

$\alpha*$ = inclination of linear slip plane to the horizontal;

γ = unit weight of the soil;

γ^p = engineering plastic shear strain;

γ_c^p = strain softening parameter;

γ_p^p = γ^p required to mobilize ϕ';

$\Delta\gamma^p$ = plastic strain increment;

$\dot{\epsilon}_{ij}^p$ = plastic deviatoric strain rate tensor;

μ = friction coefficient between pipe and soil;

μ_I = interface friction coefficient based on equivalent friction angle;

ν = Poisson’s ratio;

θ = angle of upward displacement for $\nu \neq 0$

ϕ' = mobilized angle of internal friction;

ϕ' = angle of internal friction;

ϕ'_e = equivalent friction angle;

ϕ'_{in} = ϕ' at the start of plastic deformation;

ϕ'_p = peak friction angle;

ϕ'_c = critical friction angle;

ϕ_μ = pipe–soil interface friction angle ;

ψ = mobilized dilation angle;

ψ_p = peak dilation angle;

4.15 References

Ahmed, S.M.U. (1973). “A study of the influence of confining pressure on the behaviour of sands.” M.Sc. Thesis, McGill University, Montreal, Canada.

ALA (American Lifelines Alliance). (2005). “Guidelines for the design of buried steel pipe.” Accessed July 13, 2019.

Audibert, J.M.E., and Nyman, K.J. (1977). “Soil restraint against horizontal motion of pipes.” *J. of the Geotech. Eng. Div.* ASCE, 103(NGT10), 1119–1142.

Baum, R. L., Galloway, D. L., and Harp, E. L. (2008). “Landslide and land subsidence hazards to pipelines.” *Open-File Report 2008-1164*, 192.

Bolton, M. D. (1986). “The strength and dilatancy of sands.” *Géotechnique*, 36(1), 65−78.

Calvetti, F., Di Prisco, C., and Nova, R. (2004). “Experimental and numerical analysis of soil–pipe interaction.” *J. of Geotech. and Geoenv. Eng.*, 130(12), 1292–1299.

Cheuk, C. Y., D. J. White, and M. D. Bolton. (2008). “Uplift mechanisms of pipes buried in sand.” *J. Geotech. Geoenv. Eng.*, 134 (2), 154–163.

Cocchetti, G., di Prisco, C., Galli, A., and Nova, R. (2009). “Soil–pipeline interaction along unstable slopes: a coupled three-dimensional approach. Part 1: Theoretical formulation.” *Can. Geotech. J.*, 46(11), 1289-1304.

Dafalias, Y. F., and Herrmann, L. R. (1982). “Bounding surface formulation of soil plasticity.” *Soil Mechanics–Transient and Cyclic Loads*, Pande, G. N. and Zienkiewicz, O. C., Eds., John Wiley and Sons, New York, NY., 253−282.

Dassault Systèmes. (2010). *ABAQUS* [computer program]. Dassault Systèmes, Inc., Providence, R.I.

Dickin, E. A., and Leung, C. F. (1983). “Centrifuge model tests on vertical anchor plates.” *J. Geotech. Eng.*, 12(1503), 1503–1525.

di Prisco, C., and Galli, A. (2006). “Soil-pipe interaction under monotonic and cyclic loads: experimental and numerical modelling.” *Proceedings of the First Euro Mediterranean Symposium in Advances on Geomaterials and Structures*, (c), 755–760.

EGIG (2018). “Gas pipeline incidents”. European Gas Pipeline Incident Data Group. 10th Report of the European Gas Pipeline Incident Data Group.

Fenza, G. (2016). “Experimental and numerical investigations to assess the behaviour of a buried pipeline in areas with high geological instability.” Doctoral thesis, University of Calgary.

Girgin, S., and Krausmann, E. (2015). “Lessons learned from oil pipeline natech accidents and recommendations for natech scenario development”. *JRC Science and Policy Report*, EUR 26913 EN.

Gottardi, G., and Butterfield, R. (1995). “The displacement of a model rigid surface footing on dense sand under general planar loading.” *Soils and Found.*, 35(3), 71–82.

Guo, P. (2005). “Numerical modeling of pipe–soil interaction under oblique loading.” *J. of Geotech. Geoenv. Eng.*, 131(2), 260–268.

Guo, P., and Stolle, D. (2005). “Lateral pipe-soil interaction in sand with reference to scale effect.” *J. of Geotech. Geoenv. Eng.*, 131(3), 338−349.

Hsu, T.W. (1996). “Soil restraint against oblique motion of pipelines in sand.” *Can. Geotech. J.*, 33(1), 180–188.

Hsu, T.W., Chen, Y.J., and Hung, W.Y. (2006). “Soil restraint to oblique movement of buried pipes in dense sand.” *J. of Trans. Eng.*, 132(2), 175–181.

Jung, J. K., T. D. O’Rourke, and N. A. Olson. (2013). “Uplift soil-pipe interaction in granular soil.” *Can. Geotech. J.*, 50 (7), 744–753.

Jung, J.K., O’Rourke, T.D. and Argyrou, C. (2016). “Multi-directional force–displacement response of underground pipe in sand.” *Can. Geotech. J.*, 53(11), 1763–1781.

Kouretzis, G. P., Krabbenhøft, K., Sheng, D., and Sloan, S. W. (2014). “Soil-buried pipeline interaction for vertical downwards relative offset.” *Can. Geotech. J.*, 51(10), 1087–1094.

Loukidis, D. and Salgado, R. (2011). “Effect of relative density and stress level on the bearing capacity of footings on sand.” *Géotechnique*, 61(2), 107–119.

Meyerhof, G. G. (1973). “Uplift resistance of inclined anchors and piles.” In *Proc. 8th ICSMFE*. Vol. 2, 167–172.

Monroy-Concha, M. (2013). “Soil restraints on steel buried pipelines crossing active seismic faults.” Doctoral dissertation, University of British Columbia.

Nyman, K. J. (1984). “Soil response against oblique motion of pipes.” *J. of Trans. Eng.*, 110(2), 190−202.

Pradhan, T. B. S., F. Tatsuoka, and N. Horii. (1988). “Strength and deformation characteristics of sand in torsional simple shear.” *Soils Found.*, 28(3), 131–148.

Pipeline Research Council International (PRCI) (2009). “Guidelines for constructing natural gas and liquid hydrocarbon pipelines through areas prone to landslide and subsidence hazards.” Pipeline Research Council International.

Pipeline Research Council International (PRCI) (2017). “Guidelines for constructing natural gas and liquid hydrocarbon pipelines through areas prone to landslide and subsidence hazards.” Pipeline Research Council International.

Rowe, R.K. and Davis, E.H. (1982). “Behaviour of anchor plates in sand.” *Géotechnique*, 32(1), 25–41.

Roy, K., Hawlader, B.C., Kenny, S. and Moore, I. (2016). “Finite element modeling of lateral pipeline−soil interactions in dense sand.” *Can. Geotech. J.*, 53(3), 490–504.

Roy, K., Hawlader, B.C., Kenny, S. and Moore, I. (2018a). "Upward Pipe–Soil interaction for shallowly buried pipelines in dense sand." *J. Geotech. Geoenv. Eng.*, ASCE, 144(11), 04018078.

Roy, K., Hawlader, B.C., Kenny, S. and Moore, I. (2018b). "Lateral Resistance of Pipes and Strip Anchors Buried in Dense Sand." *Can. Geotech. J.*, 55(12), 1812–1823.

Roy, K., Hawlader, B., Kenny, S., & Moore, I. (2018c). "Uplift failure mechanisms of pipes buried in dense sand." *Int. J. of Geomech.*, 18(8), 04018087.

Trautmann, C. 1983. "Behavior of pipe in dry sand under lateral and uplift loading." Ph.D. thesis, School of Civil and Environmental Engineering, Cornell Univ.

Turner, J. P., and Kulhawy, F. H. (1987). "Experimental analysis of drilled shaft foundations subjected to repeated axial loads under drained conditions." Cornell Univ., Ithaca, NY (USA). Geotechnial Engineering Group; Electric Power Research Inst., Palo Alto, CA (USA). No. EPRI-EL-5325

Turner, J.E. (2004). "Lateral force–displacement behavior of pipes in partially saturated sand." M.S. Thesis, Cornell University, Ithaca, NY.

Vesic, A. S. (1969). "Breakout Resistance of Objects Embedded in Ocean Bottom." *J. of the Soil Mech. and Found. Eng. Div.*, ASCE, Vol. 97, No. SM9, 1183–1205.

Wang, J., R. Ahmed, S. K. Haigh, N. I. Thusyanthan, and S. Mesmar. (2010). "Uplift resistance of buried pipelines at low cover–diameter ratios." In *Proc., Offshore Technology Conference*. Houston: Offshore Technology Conference.

Wang, J., S. K. Haigh, G. Forrest, and N. I. Thusyanthan. (2012). "Mobilization distance for upheaval buckling of shallowly buried pipelines." *J. Pipeline Syst. Eng. Pract.*, 3 (4), 106–114.

White, D.J., Cheuk, C.Y, and Bolton, M.D. (2008). "The Uplift resistance of pipes and plate anchors buried in sand." *Géotechnique*, 58(10), 771–779.

Wijewickreme, D., Karimian, H. and Honegger, D. (2009). “Response of buried steel pipelines subjected to relative axial soil movement.” *Can. Geotech. J.*, 46(7), 735–752.

Wijewickreme, D., Monroy, M., Honegger, D. G., and Nyman, D. J. (2017). “Soil restraints on buried pipelines subjected to reverse-fault displacement.” *Can. Geotech. J.*, 54(10), 1472–1481.

Yimsiri, S., Soga, K., Yoshizaki, K., Dasari, G., and O'Rourke, T. (2004). “Lateral and upward soil–pipeline interactions in sand for deep embedment conditions.” *J. Geotech. Geoenv. Eng.*, 130(8), 830−842.

Yoshimine, M. (2005). “Archives–soil mechanics laboratory.” Tokyo Metropolitan University,

Zhang, J., Stewart, D.P. and Randolph, M.F. (2002). “Modeling of shallowly embedded offshore pipelines in calcareous sand.” *J. of Geotech. and Geoenv. Eng*., 128(5), 363–371.

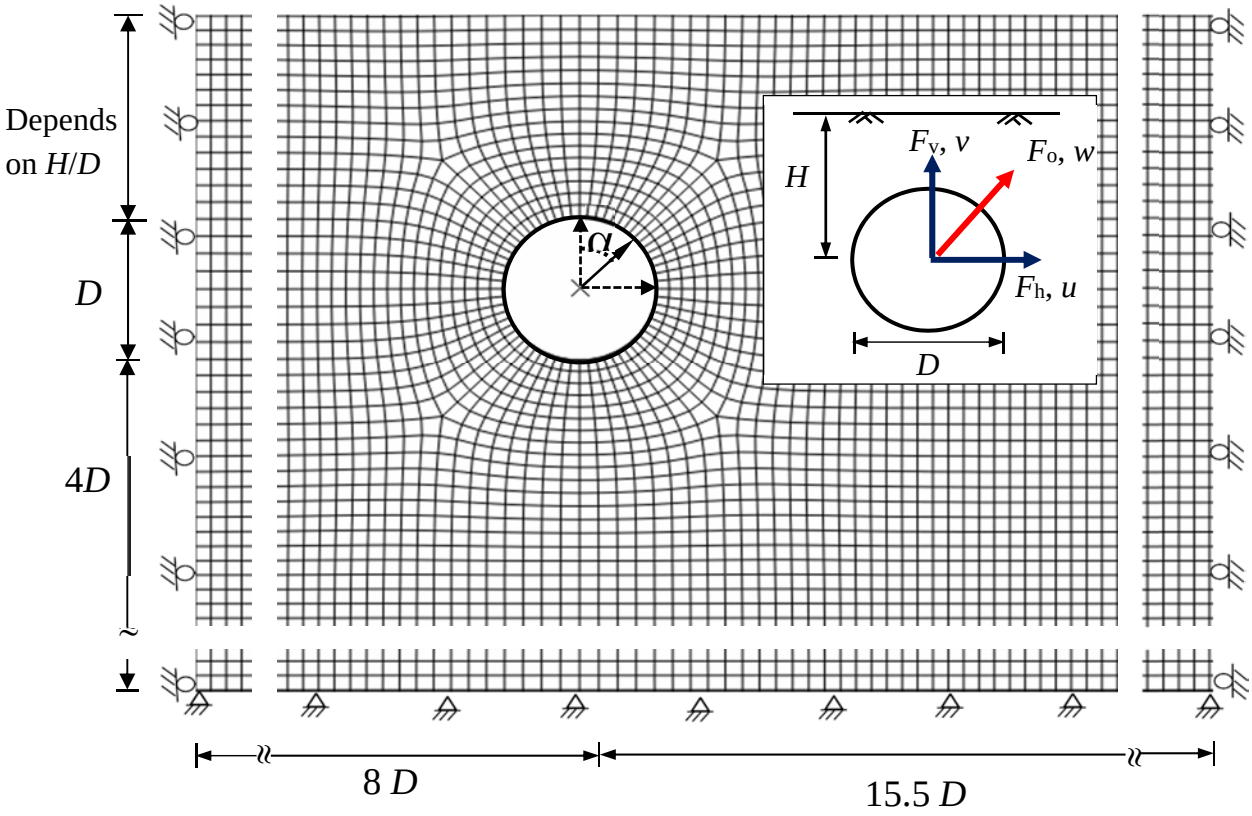

Figure 4.1 Typical finite element mesh for D = 200 mm

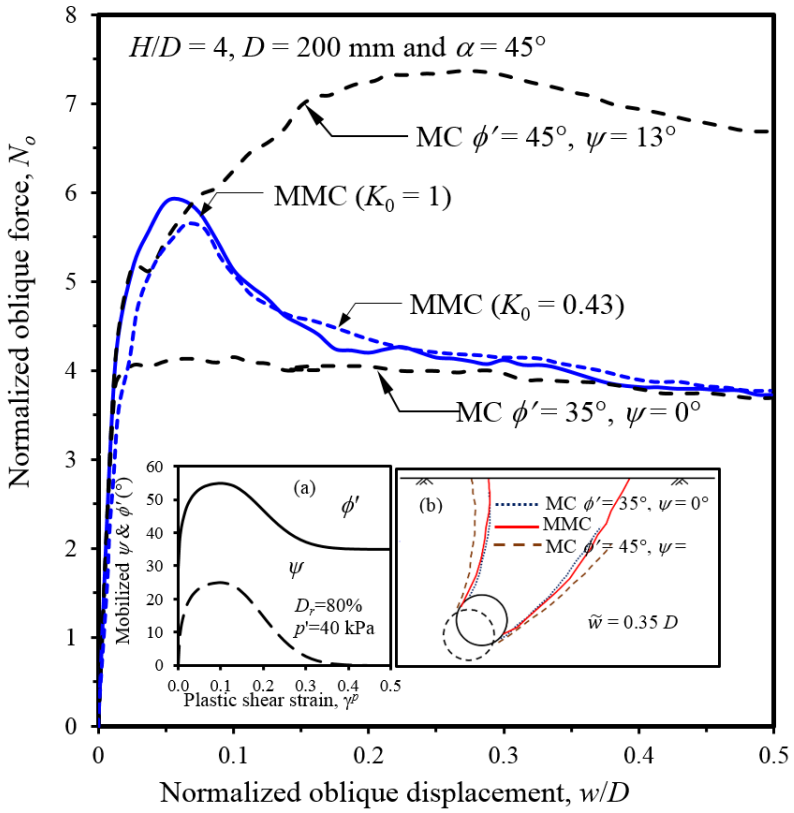

Figure 4.2 Oblique force–displacement behavior with Mohr–Coulomb and modified Mohr–Coulomb models

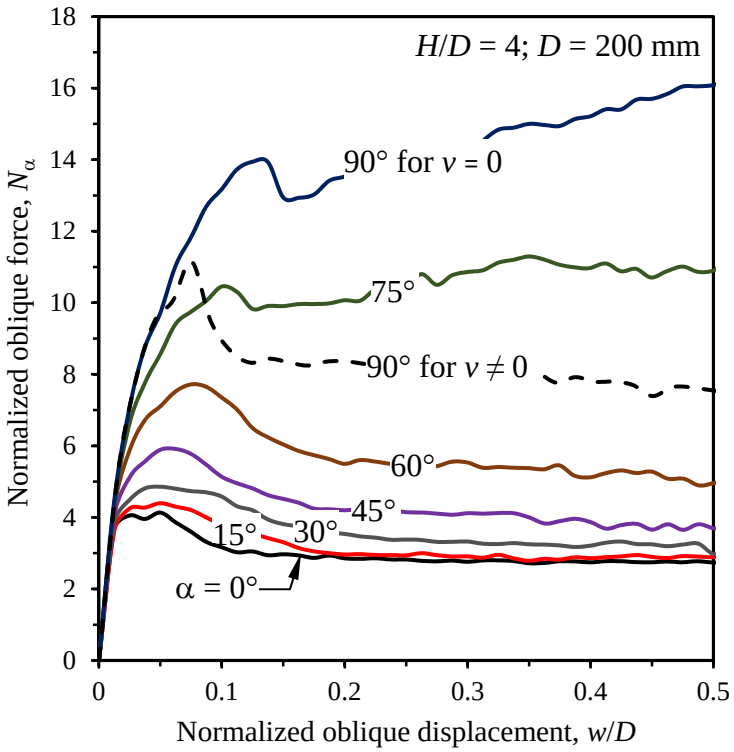

Figure 4.3 Force–displacement curves for varying oblique loading angle

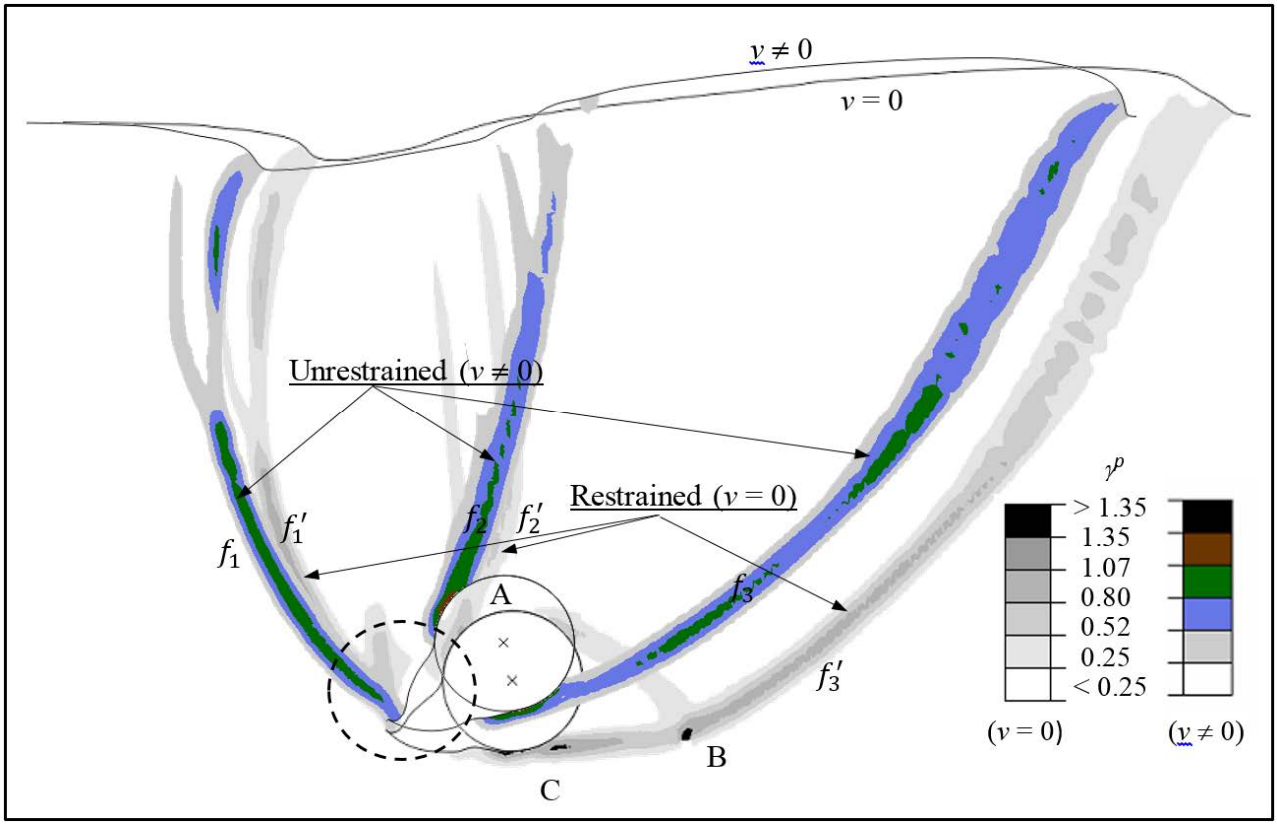

Figure 4.4 Failure mechanism for vertically restrained and unrestrained lateral loading (H/D = 4, D = 200 mm and $\widetilde{w}$ = 0.48D)

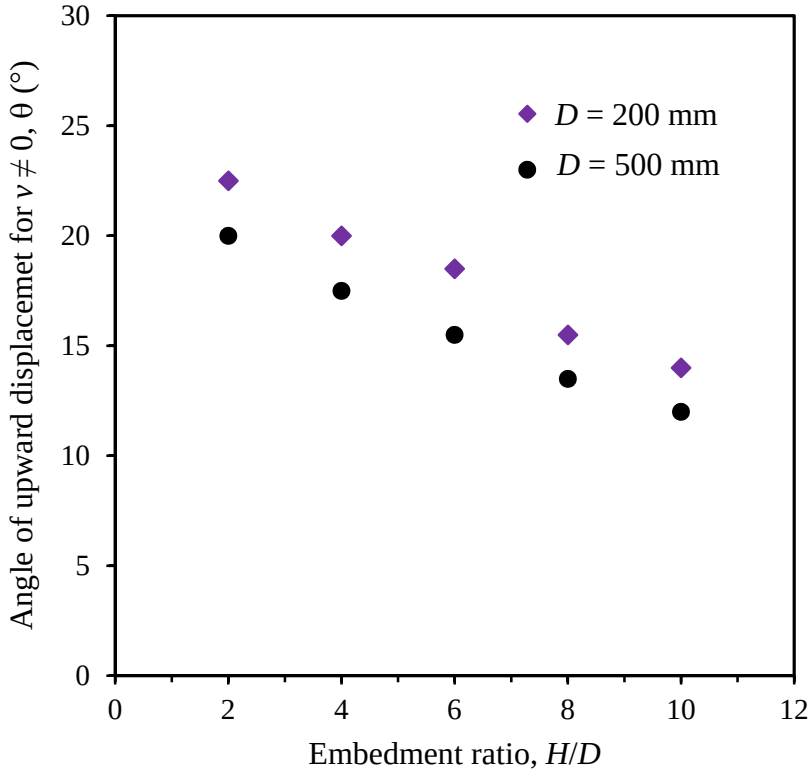

Figure 4.5 Upward pipe displacement angle for unrestrained lateral loading

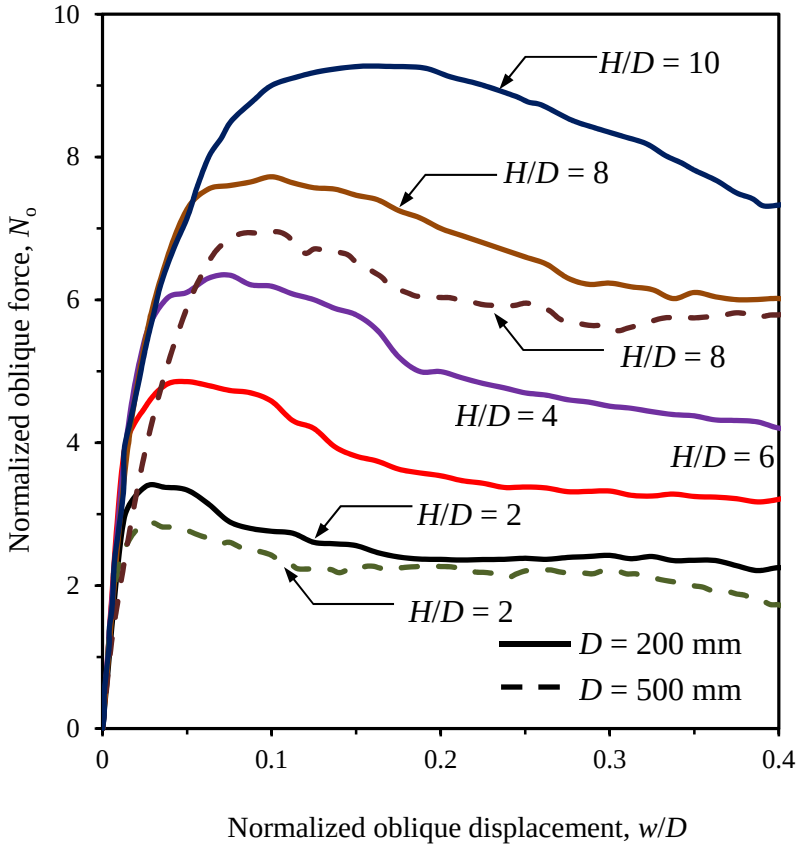

Figure 4.6 Effects of embedment ratio on force–displacement behaviour (D = 200 mm, α = 30°)

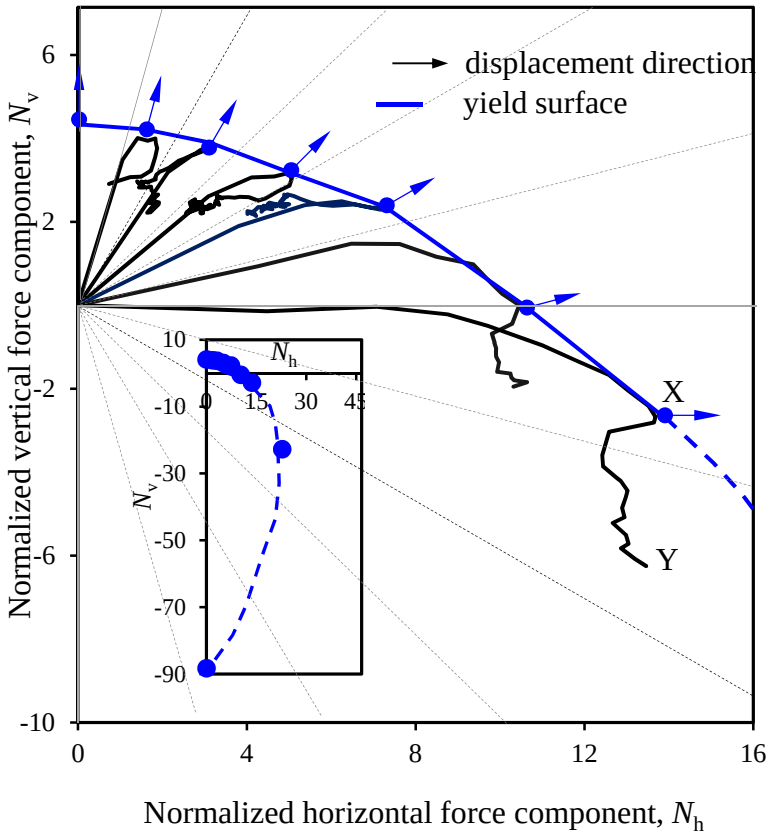

Figure 4.7 Load and displacement paths for varying oblique angle

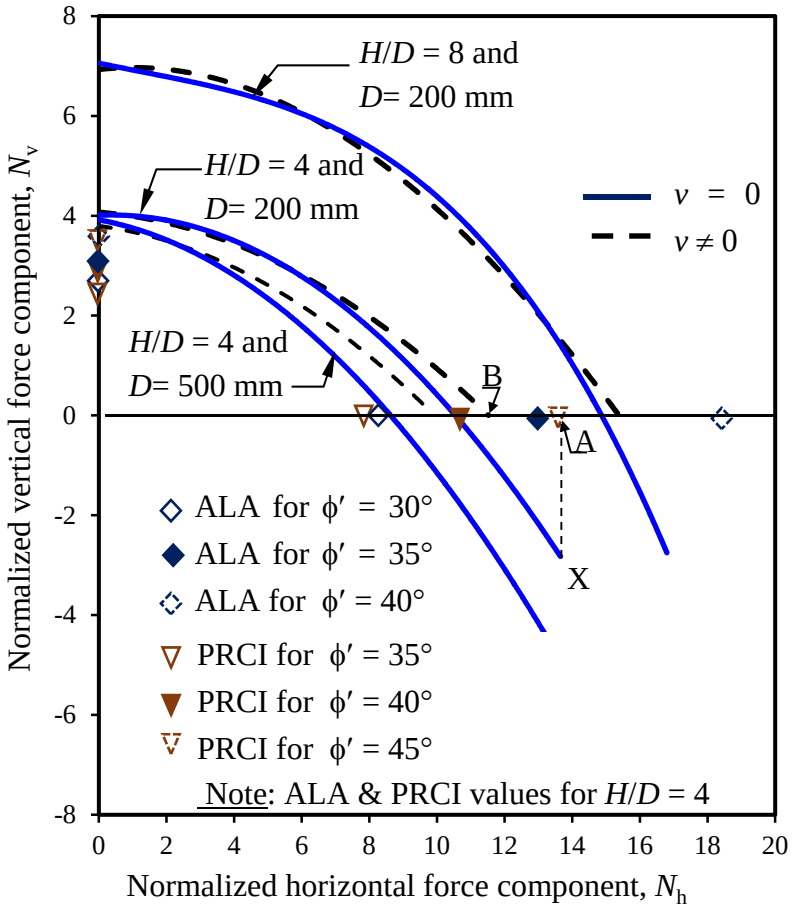

Figure 4.8 Yield envelopes for varying pipe diameter and embedment ratio

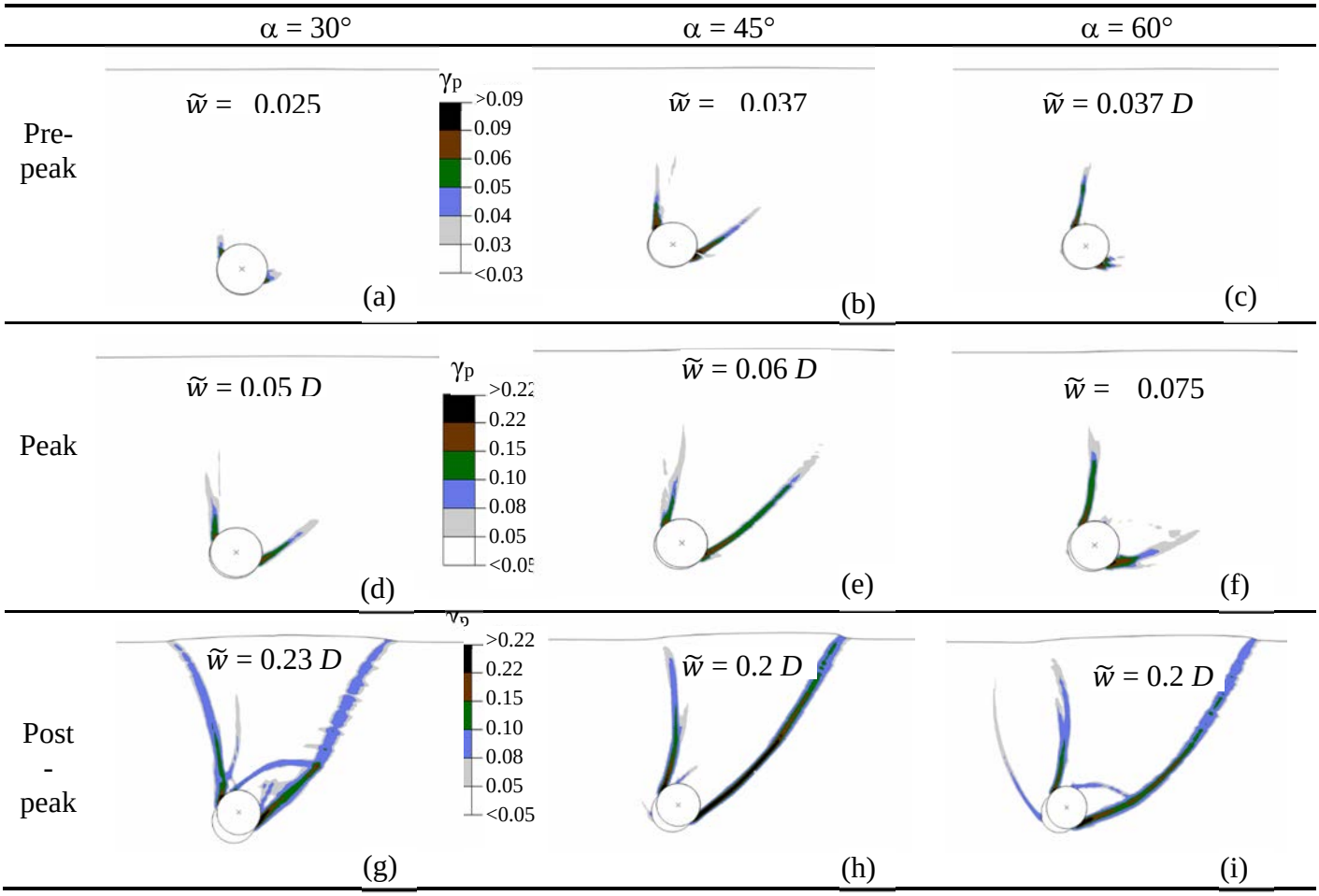

Figure 4.9 Failure mechanisms for different oblique angles (H/D = 4 and D = 200 mm)

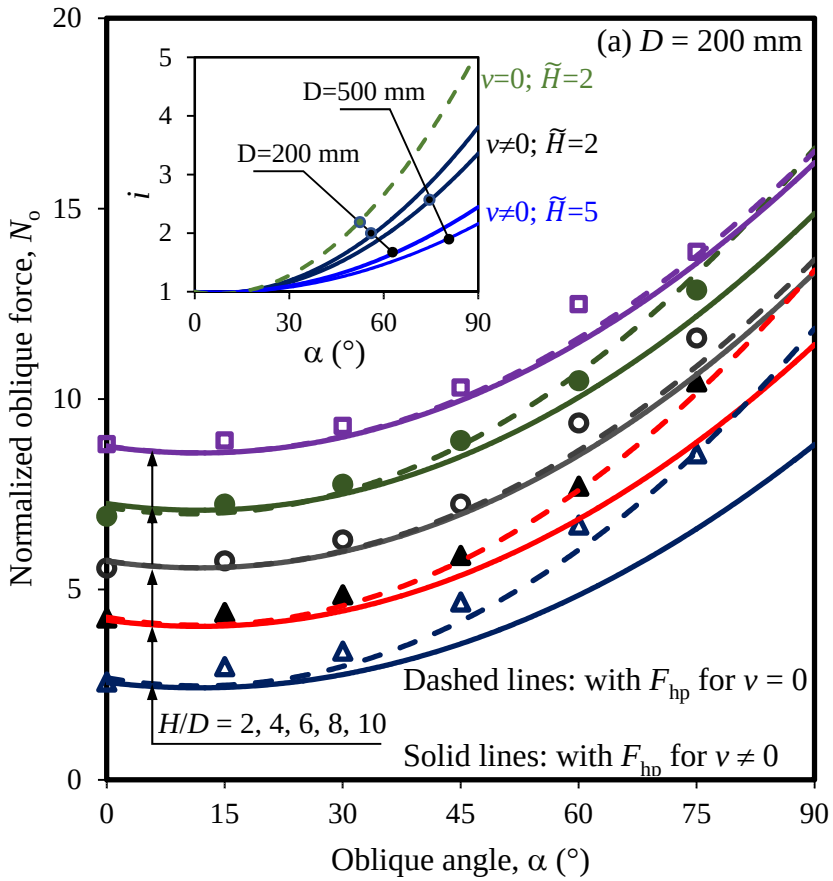
(a) D = 200 mm
Normalized oblique force, N_o
Oblique angle, α (°)
0
5
10
15
20
0
15
30
45
60
75
90
i
α (°)
1
2
3
4
5
0
30
60
90
D=500 mm
D=200 mm
v=0; $\tilde{H}$=2
v≠0; $\tilde{H}$=2
v≠0; $\tilde{H}$=5
Dashed lines: with F_{hp} for v = 0
Solid lines: with F_{hp} for v ≠ 0
H/D = 2, 4, 6, 8, 10

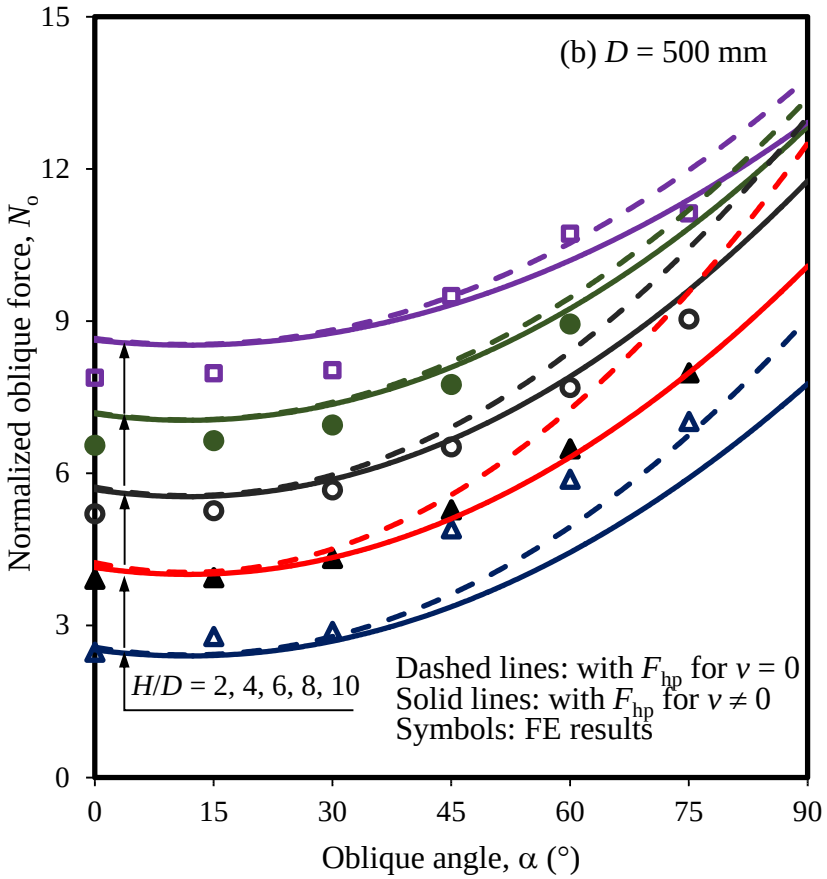

Figure 4.10 Comparison of maximum oblique forces between FEM and simplified equations: (a) D = 200 mm, (b) D = 500 mm

Table 4.1 Equations for Modified Mohr–Coulomb Model (MMC) (summarized from Roy et al. 2016)

Description	Constitutive Equations
Relative density index	$I_R=I_D(Q\text{-}\ln p')\text{-}R$ where $I_D = D_r$ (%)/100 and $0 \le I_R \le 4$
Peak friction angle	$\phi'_p - \phi'_c = A_\psi I_R$
Peak dilation angle	$\psi_p = \frac{\phi'_p - \phi'_c}{k_\psi}$
Strain softening parameter	$\gamma_c^p = C_1\text{-}C_2 I_D$
Plastic shear strain at ϕ'_p	$\gamma_p^p = \gamma_c^p \left(\frac{p'}{p'_a}\right)^m$
Pre-peak ϕ'	$\phi' = \phi'_{in} + \sin^{-1}\left[\left(\frac{2\sqrt{\gamma^p \gamma_p^p}}{\gamma^p + \gamma_p^p}\right)\sin(\phi'_p - \phi'_{in})\right]$
Pre-peak ψ	$\psi = \sin^{-1}\left[\left(\frac{2\sqrt{\gamma^p \gamma_p^p}}{\gamma^p + \gamma_p^p}\right)\sin(\psi_p)\right]$
Post-peak ϕ'	$\phi' = \phi'_c + \left(\phi'_p - \phi'_c\right)\exp\left[-\left(\frac{\gamma^p - \gamma_p^p}{\gamma_c^p}\right)^2\right]$
Post-peak ψ	$\psi = \psi_p \exp\left[-\left(\frac{\gamma^p - \gamma_p^p}{\gamma_c^p}\right)^2\right]$
Young's modulus	$E = K p'_a \left(\frac{p'}{p'_a}\right)^n$

Table 4.2 Geometry and soil properties used in FE analyses

Parameter	Values
External diameter of pipe, D (mm)	200, 500
K	150
n	0.5
Atmospheric pressure, p'_a (kN/m^2)	100
Poisson's ratio of soil, ν_{soil}	0.2
A_ψ	5
k_ψ	0.8
Initial angle of internal friction, ϕ'_{in} (°)	29
C_1	0.22
C_2	0.11
m	0.25
Critical state of friction angle, ϕ'_c (°)	35
Relative density, D_r (%)	80
Dry unit weight of soil, γ (kN/m^3)	17.7
Interface friction coefficient, μ	0.32
Embedment ratio, H/D	2, 4, 6, 8, 10

Note: A small cohesion of 0.5 kPa is used to avoid numerical issues although $c' = 0$ for sand

Chapter 5
Conclusions and Recommendations for Future Research

5.1 Conclusions

The response of buried pipelines under oblique loading is an important engineering consideration for safe and economical design and operation of pipelines. In this thesis, the soil restraint of the pipelines buried in dense sand is studied for the oblique motion of pipelines in the vertical (upward)–horizontal plane. As the thesis has been prepared in manuscript format, the problem-specific conclusions are presented at the end of Chapters 3 and 4. The following are the overall summary and general conclusions.

- The modified Mohr–Coulomb (MMC) model shows a better performance than the traditional Mohr–Coulomb (MC model) to simulate the observed behavior of buried pipelines in dense sand subjected to oblique loading in physical model tests. More specifically, it can simulate the post-peak degradation of soil resistance at large displacements. The MMC model considers the variation of angles of internal friction and dilation with plastic shear strain, loading condition, density and confining pressure, as observed in laboratory tests on dense sand. The consideration of the pre-peak hardening and post-peak softening behavior of dense sand in the MMC model can also capture the initiation and propagation of shear bands and thereby soil failure mechanisms.
- The effects of restrained and unrestrained loading conditions on force–displacement behavior is highlighted. For example, the restraint to vertical movement during lateral loading increases the lateral resistance as compared to unrestrained loading cases. The effects of restrainted

pipe displacement is more significant for shallow burial depths. The force–displacement response is not affected by the restrained/unrestrained condition for pure vertical loading.

- The finite element analyses show that the load and displacement paths do not coincide, which represents a non-associated loading condition. For the displacement-controlled loading, the load-path after generation of plastic shear strains is significantly influenced by the formation and propagation of shear bands.
- Nyman's (1984) inclination factor can be used to estimate the maximum oblique force providing the maximum lateral and vertical soil restraints are properly selected.

5.2 Recommendations for Future Research

The numerical analyses presented in this thesis show that many important features observed in physical experiments can be simulated using the present finite element modeling approach. However, there are some limitations which could be studied further.

- The response of pipeline buried in dense sand is studied in this thesis. However, in many practical situations, the soil around the pipeline is loose to medium dense, which could be studied by developing appropriate soil models for this type of sand.
- A detailed parametric study could be performed for varying embedment ratio, pipe diameter and soil properties.
- The analyses presented in this thesis is limited to only the vertical (upward)–lateral oblique loading cases. The response of pipeline in other oblique loading conditions could be studied.
- Generally the backfill soil in the trench is different from the native soil. The trench effect on pipeline response could be studied.

References

American Lifelines Alliance (ALA). (2005). “Guidelines for the Design of Buried Steel Pipe.” <https://www.americanlifelinesalliance.com/pdf/Update061305.pdf > (Accessed Jul. 27, 2019).

Audibert, J.M.E., and Nyman, K.J. (1977). “Soil restraint against horizontal motion of pipes.” *J. of the Geotech. Eng. Div. ASCE*, 103(NGT10), 1119–1142.

Bhattacharya, P., and Kumar, J. (2013). “Seismic pullout capacity of vertical anchors in sand.” Geomech. and Geoeng., 8(3),191–201.

Burnett, A. (2015). “Investigation of full scale horizontal pipe-soil interaction and large strain behaviour of sand.” M.A.Sc. thesis, Queen's University, Canada.

Calvetti, F., Di Prisco, C., and Nova, R. (2004). “Experimental and numerical analysis of soil–pipe interaction.” *J. of Geotech. and Geoenv. Eng.*, 130(12), 1292–1299.

Cheuk, C. Y., White, D. J. and Bolton, M. D. 2008. “Uplift Mechanisms of Pipes Buried in Sand.” *J. of Geotech. and Geoenv. Eng.*, 134(2), 154–163.

Chin, E. L., Craig, W. H., and Cruickshank, M. (2006). “Uplift resistance of pipelines buried in cohesionless soil.” *Proc., 6th Int. Conf. on Phy. Model. in Geotech.*, Ng, Zhang, and Wang, eds., Vol. 1, Taylor and Francis Group, London, 723–728.

Clukey, E.C., Haustermans, L. and Dyvik, R. (2005). “Model tests to simulate riser–soil interaction effects in touchdown point region.” *Proc., International Symposium on Frontiers in Offshore Geotechnics (ISFOG 2005)*, Perth, Australia, 651–658.

Cocchetti, G., di Prisco, C., Galli, A., and Nova, R. (2009). “Soil–pipeline interaction along unstable slopes: a coupled three-dimensional approach. Part 1: Theoretical formulation.” *Can. Geotech. J.*, 46(11), 1289-1304.

Daiyan, N., Kenny, S., Phillips, R. and Popescu, R. (2011). “Investigating pipeline–soil interaction

under axial–lateral relative movements in sand." *Can. Geotech. J.*, 48(11): 1683–1695.

Daiyan, Nasser. (2013). "Investigating soil/pipeline interaction during oblique relative movements." PhD thesis, Memorial University of Newfoundland.

Debnath, P. (2016). "Centrifuge modeling of oblique pipe-soil interaction in dense and loose sand." M.Eng. thesis, Memorial University of Newfoundland.

Dickin, E.A., and King, G.J.W. (1993). "Finite element modelling of vertical anchor walls in sand." *Developments in Civil & Construction Engineering Computing*, Civil-Comp Press, Edinburgh, UK, 171–181.

Di Prisco, C. and Galli, A. (2006). "Soil-pipe interaction under monotonic and cyclic loads: experimental and numerical modelling." *In Proceedings of the First Euro Med. Symposium on Advances in Geomaterials and Structures*, Hammamet, Tunisia. pp. 755–760.

DNV 2007 (Det Norske Veritas). DNV-OS-F101. Available from: https://exchange.dnv.com/servicedocuments/dnv/ [accessed 4 April 2019].

Eidinger, J., O'Rourke, M., and Bachhuber, J. 2002. "Performance of pipelines at fault crossings." *7th U.S. National Conf. of Earth. Eng.* Earthquake Engineering Research Institute, El Cerrito, Calif.

Farhadi Hikooei, B. (2013). "Numerical modeling of pipe-soil interaction under transverse direction." Doctoral thesis, University of Calgary.

Fenza, G. (2016). "Experimental and numerical investigations to assess the behaviour of a buried pipeline in areas with high geological instability." Doctoral thesis, University of Calgary.

Ha, D., Abdoun, T.H., O'Rourke, M.J., Symans, M.D., O'Rourke, T.D., Palmer, M.C., and Stewart, H.E. (2008). "Centrifuge modeling of earthquake effects on buried high-density polyethylene (HDPE) pipelines crossing fault zones." *J. of Geotech. and Geoenv. Eng* , 134(10), 1501–1515.

Hodder, M.S., and Cassidy, M.J. (2010). "A plasticity model for predicting the vertical and lateral

behaviour of pipelines in clay soils." *Géotechnique*, 60(4), 247–263.

Hsu, T.W. (1996). "Soil restraint against oblique motion of pipelines in sand." *Can. Geotech. J.*, pp. 180–188.

Hsu, T.W., Chen, Y.J., and Wu, C.Y. (2001). "Soil friction restraint of oblique pipelines in loose sand." *J. of Trans. Eng.*, 127(1), 82–87.

Hsu, T.W., Chen, Y.J. and Hung, W.C. (2006). "Soil restraint to oblique movement of buried pipes in dense sand." *J. of Trans. Eng.*132(2): 175–181.

Jung, J.K., O'Rourke, T.D. and Argyrou, C. (2016). "Multi-directional force–displacement response of underground pipe in sand." *Can. Geotech. J.*, 53(11), 1763–1781.

Marcotte, G. (2018). "Centrifuge Modeling of Lateral-Axial Oblique Loading on Buried Pipelines in Cohesionless Soil." Doctoral thesis, Carleton University.

Meyerhof, G. G. (1973). "Uplift resistance of inclined anchors and piles." In *Proc. 8th ICSMFE*. Vol. 2, 167–172.

Monroy-Concha, M. (2013). "Soil restraints on steel buried pipelines crossing active seismic faults." Doctoral thesis, University of British Columbia.

Nyman, K. J. (1984). "Soil response against oblique motion of pipes." *J. of Trans. Eng.*, 110(2), 190-202.

Pike, K. and Kenny, S. (2011). "Advancement of CEL procedures to analyze large deformation." In *Off. Techn. Conf.*, Paper no. 22004.

Pike, K. (2016). "Physical and numerical modelling of pipe/soil interaction events for large deformation geohazards." PhD thesis, Memorial University of Newfoundland, St. John's, Canada.

Pipeline Research Council International (PRCI) (2009). "Guidelines for constructing natural gas and liquid hydrocarbon pipelines through areas prone to landslide and subsidence hazards." Pipeline

Research Council International.

Randolph, R.F. (2012). “Offshore geotechnics–the challenges of deepwater soft sediments.” *In Proc., GeoCongress 2012*, March 25–29, California, USA, 241–371.

Rowe, R.K. and Davis, E.H. (1982). “Behaviour of anchor plates in sand.” *Géotechnique*, 32(1), 25–41.

Roy, K.S., and Hawlader, B. (2012). “Soil restraint against lateral and oblique motion of pipes buried in dense sand.” *In Proc. 9th International Pipeline Conference*. American Society of Mechanical Engineers. pp. 7–12.

Roy, K., Hawlader, B.C., Kenny, S. and Moore, I. (2016). “Finite Element Modeling of Lateral Pipeline−Soil Interactions in Dense Sand.” *Can. Geotech. J.*, 53(3), 490–504.

Roy, K., Hawlader, B.C., Kenny, S. and Moore, I. (2018a). “Upward Pipe–Soil interaction for shallowly buried pipelines in dense sand.” *J. of Geotech. and Geoenv. Eng* , ASCE, 144(11), 04018078.

Roy, K., Hawlader, B.C., Kenny, S. and Moore, I. (2018b). “Lateral Resistance of Pipes and Strip Anchors Buried in Dense Sand.” *Can. Geotech. J.*, 55(12), 1812–1823.

Stuyts, B., Cathie, D., and Powell, T. (2016). “Model uncertainty in uplift resistance calculations for sandy backfills.” *Can. Geotech. J.*, 53(11), 1831–1840.

Trautmann, C. (1983). “Behavior of pipe in dry sand under lateral and uplift loading.” PhD thesis, Cornell University, Ithaca, NY.

Vesic, A. S. (1969). “Breakout Resistance of Objects Embedded in Ocean Bottom.” *J. of the Soil Mech. and Found. Eng. Div.,* ASCE, Vol. 97, No. SM9, 1183–1205.

White, D. J., Cheuk, C. Y., and Bolton, M. D. (2008). “The uplift resistance of pipes and plate anchors buried in sand.” *Géotechnique*, 58(10), 771–777.

Wijewickreme, D., Monroy, M., Honegger, D. G., and Nyman, D. J. (2017). “Soil restraints on buried pipelines subjected to reverse-fault displacement.” *Can. Geotech. J.*, 54(10), 1472–1481.

Yimsiri, S., Soga, K., Yoshizaki, K., Dasari, G., and O'Rourke, T. (2004). “Lateral and upward soil–pipeline interactions in sand for deep embedment conditions.” *J. of Geotech. and Geoenv. Eng*., 130(8), 830−842.

Yu, S.B., Hambleton, J.P., and Sloan, S.W. (2014). “Analysis of inclined strip anchors in sand based on the block set mechanism.” *In Applied Mechanics and Materials. Trans Tech* Publications, Vol. 553, 422–427.

Zhang, J., Stewart, D.P. and Randolph, M.F. (2002). “Modeling of shallowly embedded offshore pipelines in calcareous sand.” *J. of Geotech. and Geoenv. Eng*., 128(5), 363–371.